

Chapter 1

Black hole-neutron star binaries

Matthew D. Duez

Abstract The gravitational wave signals of black hole-neutron star (BHNS) binary systems have now been detected, and future detections might be accompanied by electromagnetic counterparts. BHNS mergers involve much of the same physics as binary neutron star mergers: strong gravity, nuclear density matter, neutrino radiation, and magnetic turbulence. They also share with binary neutron star systems the potential for bright electromagnetic signals, especially gamma ray bursts and kilonovae, and the potential to be significant sources of r-process elements. However, BHNS binaries are more asymmetric, and their mergers produce different amounts and arrangements of the various post-merger material components (e.g. disk and dynamical ejecta), together with a more massive black hole; these differences can have interesting consequences. In this chapter, we review the modeling of BHNS mergers and post-merger evolution in numerical relativistic hydrodynamics and magnetohydrodynamics. We attempt to give readers a broad understanding of the answers to the following questions. What are the main considerations that determine the merger outcome? What input physics must (or should) go into a BHNS simulation? What have the most advanced simulations to date learned?

1.1 Introduction

Black hole-neutron star (BHNS) binary inspirals and mergers involve extremes of all four fundamental forces; they involve strong, dynamical spacetime curvature, supra-nuclear matter densities, relativistic speeds, powerful neutrino emission and magnetic field production. They are strong sources of gravitational waves. In some cases, they might also produce bright electromagnetic signals via kilonovae and/or gamma ray bursts and be a significant site for the production of heavy elements. Un-

Matthew Duez (✉)

Department of Physics & Astronomy, Washington State University, Pullman, Washington 99164, USA, e-mail: m.duez@wsu.edu

til recently, they were known to us only by theory, their rate of occurrence a matter of loosely-constrained speculation, with no observational data. Now that has changed.

On Jan 5, 2020, during the LIGO O3 observing run, LIGO Livingston registered a gravitational wave signal, designated GW200105, consistent with the late inspiral of a BHNS binary. (LIGO Hanford was not operational at the time.) Ten days later, LIGO Hanford, LIGO Livingston, and Virgo coincidentally detected another gravitational wave signal, GW200115, also consistent with a BHNS inspiral [1]. The two signals were reported together, although GW200115 was the far more confident detection; in fact, GW200105 was later downgraded to a “marginal candidate” [2]. The other possible BHNS detections GW190917 and GW191219 were also reported in O3 catalog papers [3, 2, 4].

The identification of these binaries as BHNS systems was based entirely on the inferred masses of the binary components. From GW200105 was inferred a primary mass of $M_1 = 8.9^{+1.2}_{-1.5} M_\odot$ and a secondary mass of $M_2 = 1.9^{+0.3}_{-0.2} M_\odot$. From GW200115 was inferred a primary mass of $M_1 = 5.7^{+1.8}_{-2.1} M_\odot$ and a secondary mass of $M_2 = 1.5^{+0.7}_{-0.3} M_\odot$. For GW191219, the masses were $M_1 = 31.1^{+2.2}_{-2.7} M_\odot$, $M_2 = 1.17^{+0.07}_{-0.06} M_\odot$; for GW190917, $M_1 = 9.7^{+3.4}_{-3.9} M_\odot$, $M_2 = 2.1^{+1.1}_{-0.4} M_\odot$. The maximum mass of a non-spinning neutron star $M_{\text{NS,max}}$ is somewhere in the range 2–3.2 M_\odot , with the minimum value coming from the maximum inferred masses of observed pulsars [5, 6] and the maximum value derived from causality restrictions on the nuclear equation of state [7]. Thus, any compact object more massive than this is presumably a black hole. While black holes could exist with masses below $M_{\text{NS,max}}$, there is no known astrophysical way to form them, so compact objects with mass less than $M_{\text{NS,max}}$ are presumed to be neutron stars. The waveform also allowed LIGO-Virgo researchers to estimate a parameter related to the black hole spin, namely the effective inspiral spin parameter χ_{eff} . This is a mass-weighted average of the component parallel to the orbital angular momentum of the Kerr dimensionless spin parameter $\chi \equiv \mathbf{J}/M^2$. Thus, $\chi_{\text{eff}} = (M_1 \chi_1 + M_2 \chi_2) \cdot \hat{L} / (M_1 + M_2)$. This will most likely be dominated by the black hole’s spin. For GW200105, $\chi_{\text{eff}} = -0.01^{+0.11}_{-0.15} M_\odot$, consistent with zero, while for GW200115, $\chi_{\text{eff}} = -0.19^{+0.23}_{-0.35} M_\odot$, giving a probability of 88% that the black hole has a spin *negatively* aligned with respect to the orbital angular momentum.

The detections were a matter of excitement for the astronomy community, because before there had been no confident detections of BHNS systems through any signal type. Radio surveys which have identified binary neutron star systems in our galaxy have thus far failed to find any black hole-pulsar binaries. LIGO’s O1 and O2 observing runs found no BHNS signals. The first part of the O3 run turned up only two ambiguous signals: GW190426, which may have been a detector artifact, and GW190814, which had a secondary mass $M_2 = 2.59^{+0.08}_{-0.09} M_\odot$ and might be a binary black hole system [8, 9]. In the absence of observations, the event rate of BHNS mergers was highly uncertain. Population synthesis studies estimate it within 0.1–800 $\text{Gpc}^{-3} \text{yr}^{-1}$, and lack of detections in O1 and O2 suggested an upper bound of $< 610 \text{Gpc}^{-3} \text{yr}^{-1}$. Using two candidate detections in GWTC-3, admittedly very small number statistics, allowed the LIGO-Virgo-KAGRA collaboration to constrain the rate of BHNS mergers to between 7.8 $\text{Gpc}^{-3} \text{yr}^{-1}$ and 140 $\text{Gpc}^{-3} \text{yr}^{-1}$ [10].

We should now be optimistic that LIGO-Virgo will detect more BHNS signals as it approaches its design sensitivity. Furthermore, a subset of BHNS mergers produce potentially detectable electromagnetic counterparts, carrying information about the fascinating postmerger dynamics. The two most-studied electromagnetic signal possibilities for a BHNS merger are a *kilonova* and a *gamma ray burst* (GRB).

Kilonovae are caused by matter ejected from the merger site. As the matter decompresses, it forms unstable nuclei whose radioactive decays power a potentially detectable thermal IR/visible/UV signal lasting days. (See Section 1.9 below and the review [11].)

GRBs are non-thermal high-energy emission originating from a highly-relativistic outflow. In order to achieve the needed Lorentz factors, a large energy must be released without an accompanying large load of mass. Jets from the inner region near the black hole shooting out along the polar directions are a preferred scenario. (See Section 1.8 on the generation of these jets.) Short duration GRBs (lasting less than two seconds) are thought to have their origin in compact binary [BHNS or neutron star-neutron star (NSNS)] mergers [12], although the detection of kilonovae following a couple of ~ 10 second GRBs suggests that mergers may also sometimes produce longer-duration GRBs [13, 14]. Furthermore, many short GRBs show “extended emission” subsequent to the initial spike [15]. (For reviews of short GRBs, see [12, 16].) GRBs have higher isotropic equivalent luminosity than kilonovae ($\sim 10^{50}$ erg s^{-1} vs $\sim 10^{40}$ erg s^{-1}), but their emission is highly collimated, so the observer must be somewhat close to the axis to see it. Kilonovae, on the other hand, emit fairly isotropically and for longer times. Thus, they have different strengths and weaknesses as electromagnetic counterparts to a gravitational wave signal [17, 18]. The binary neutron star gravitational wave event GW170817 was detected as both a GRB and a kilonova [19].

Other mechanisms for electromagnetic emission have been considered and will be mentioned in later sections. Interaction of the neutron star magnetosphere with the black hole might create fast radio burst and X-ray transients (see Section 1.6). If the jet must pierce through previously-emitted ejecta, it will produce a hot surrounding cocoon, producing its own emission and affecting observations of the jet [20, 21, 22]. Outflow interacting with the surrounding interstellar medium creates radio emission (see Section 1.9).

This chapter is organized as follows. In Section 1.2, we will provide an overview of the inspiral, merger, and postmerger process. In Section 1.3, we will explore the space of possible BHNS binary systems and attempts to use numerical simulations to map properties of the pre-merger binary to the post-merger outcome. Section 1.4 presents, one piece at a time, the components of a realistic simulation of a BHNS merger. Subsequent sections summarize what has been learned from numerical simulations about the various aspects and outputs of the mergers: gravitational waves (Section 1.5), signals from the neutron star magnetosphere (Sec. 1.6), the post-merger disk (Sec. 1.7), production of magnetic fields and jets (Sec. 1.8), and outflows (Sec. 1.9).

For other excellent reviews of BHNS systems see Kyutoku *et al* [23] and Foucart [24]. Unless otherwise specified, we will use units for which $G = c = 1$ throughout this chapter.

1.2 Phases of a BHNS merger

In this section, we outline the evolution stages of a BHNS system. We introduce the main concepts that will recur throughout the chapter and provide physical arguments for what we expect simulations to find.

The most likely formation scenario for a BHNS binary begins with a binary of high-mass main sequence stars in a region of stellar density low enough that the binary evolves in isolation (a “field binary”). If one star evolves into a neutron star and the other into a black hole—and no supernova kick disrupts the binary, there will be a BHNS binary. However, only BHNS systems that merge within the age of the Universe are interesting to us. Probably this requires the binary to undergo a common envelope phase, leaving the binary sufficiently compact that gravitational radiation can bring the neutron star and black hole to merger within a Hubble time.

Consider a binary composed of a black hole of mass M_{BH} and a neutron star of mass M_{NS} in an orbit with semimajor axis D . We expect M_{BH} to be significantly larger than M_{NS} , perhaps $M_{\text{BH}} \approx 5M_{\text{NS}}$ will be typical. (See Section 1.3.) The binary will have a Keplerian orbital angular frequency $f \approx M_{\text{BH}}^{1/2} D^{-3/2}$. It will thus have a time-varying mass quadrupole moment and so will radiate gravitational waves. These waves carry away energy and angular momentum. The orbital energy of the binary in Newtonian gravity is $E = -M_{\text{BH}}M_{\text{NS}}/2D$, and this orbital energy will decrease at a rate $\dot{E} = -L_{\text{GW}}$, where L_{GW} is the gravitational radiation luminosity. One can then infer $\dot{D} = dD/dE\dot{E}$. Gravitational waves cause the eccentricity to decrease, so by the time the neutron star and black hole are close, the orbit will be very close to circular. (BHNS binaries formed by multi-body gravitational interactions in dense stellar environments such as globular clusters, on the other hand, might be very eccentric at the time of merger, but such events are expected to be much rarer than field binary BHNS mergers [25].) The inspiral rate will at first be very small, but as D decreases, the binary will orbit faster, increasing L_{GW} and causing the inspiral rate to increase. This is the inspiral phase.

Either of two effects might terminate the inspiral phase. First, the binary separation might reach the innermost stable circular orbit R_{ISCO} , inside of which orbital motion is unstable, and so the neutron star will plunge into the black hole on an orbital timescale. If $M_{\text{BH}} \gg M_{\text{NS}}$, this separation is that of test particles orbiting an isolated black hole, which depends only on M_{BH} and on the black hole’s angular momentum \mathbf{J}_{BH} . In general, the orbital and black hole spin angular momentum will not be aligned, but we shall consider this first as the simplest case. Then $R_{\text{ISCO}} = f(\chi)M_{\text{BH}}$ where $\chi = |J_{\text{BH}}|/M_{\text{BH}}^2 < 1$ is the dimensionless spin, and in Boyer-Lindquist coordinates the limits are $f(0) = 6$, $f(1) = 1$. In any case, the plunge radius R_{plunge} can be taken to be of order $\sim M_{\text{BH}}$.

Second, the neutron star might be torn apart by the tidal force of the black hole. This will happen when the tidal force from the black hole exceeds the neutron star's self-gravity. Both of these forces depend on the neutron star radius R_{NS} . From Newtonian physics, the gravitational force of a test body with mass m near the surface due to the neutron star's gravity is $\sim mM_{\text{NS}}/R_{\text{NS}}^2$ and the tidal force from the black hole (the difference in the black hole's gravitational forces for test bodies on the sides near and far from the hole) is $\sim mM_{\text{BH}}R_{\text{NS}}/D^3$. Setting the two forces equal we find the tidal mass transfer radius $D = R_{\text{tidal}}$:

$$R_{\text{tidal}} = \left(\frac{M_{\text{BH}}}{M_{\text{NS}}} \right)^{1/3} R_{\text{NS}} = M_{\text{BH}} Q^{-2/3} C^{-1} \quad (1.1)$$

where we have introduced two crucial dimensionless binary parameters: the *mass ratio* $Q \equiv M_{\text{BH}}/M_{\text{NS}}$ and the neutron star *compaction* $C \equiv M_{\text{NS}}/R_{\text{NS}}$.

Even after the neutron star begins losing mass, it persists inspiraling as a gravitationally bound compact object with most of its original mass for a short time (an orbit or so) longer before being totally disrupted. It is sometimes useful to distinguish the beginning of mass transfer off of the neutron star at $D = R_{\text{tidal}}$ from tidal disruption, when the neutron star has been torn into a spiral swath. The latter does quickly follow the former, though, so we will ignore the distinction for the rest of this section.

Tidal disruption would be expected to have a profound effect on the gravitational wave signal. By spreading the neutron star matter, the variation of the quadrupole moment will drop, and the gravitational wave will quickly damp. We can estimate this cutoff frequency, using the fact that the frequency of the dominant (quadrupolar) gravitational wave mode, f_{cut} is twice the orbital frequency. Schematically,

$$f_{\text{cut}} \sim M_{\text{BH}}^{1/2} R_{\text{tidal}}^{-3/2} \sim M_{\text{NS}}^{1/2} R_{\text{NS}}^{-3/2} \quad (1.2)$$

i.e. the cutoff frequency is mostly given by the dynamical timescale of the neutron star. This is one way that information about the neutron star is encoded in the waveform [26]. Unfortunately, f_{cut} comes to $\approx \text{kHz}$, which is well above LIGO's peak sensitivity.

Thus, we have three possible endpoints of the BHNS inspiral. If $R_{\text{plunge}} > R_{\text{tidal}}$, we have a *non-disrupting binary* whose inspiral ends with the neutron star plunging into the black hole horizon still intact. If $R_{\text{tidal}} > R_{\text{plunge}}$, we have a *disrupting binary* whose inspiral ends when the neutron star, still outside the black hole, is torn apart by the black hole's gravity. Finally, there could be marginal systems where $R_{\text{tidal}} \approx R_{\text{plunge}}$. This will be the case if

$$\zeta \equiv f(\chi) Q^{2/3} C \approx 1 \quad (1.3)$$

Disruption is expected, then, for $\zeta \lesssim 1$, which will be more likely for high black hole spin, low mass ratio (i.e. low M_{BH}), and low compaction (in particular, for large R_{NS}).

For non-disrupting BHNS binaries, one would not expect residual matter outside the black hole after the plunge, which eliminates the possibility of most sorts of electromagnetic signals. The infalling neutron star will disturb the spacetime near the horizon, leading to a distinctive “ringdown” segment of the waveform, and one would expect that to be the end of the story.

For disrupting binaries, the neutron star will elongate into a spiral, with some material expanding outward away from the black hole and some falling inward toward the black hole. We will find that, for non-eccentric BHNS binaries, mass transfer once begun is unstable, and the neutron star is always completely destroyed in a single tidal disruption event. Some of the outgoing material in the spiral has positive energy and is unbound. This *dynamical ejecta*, permanently expelled from the system, can be quite massive (10^{-2} – $10^{-1} M_{\odot}$) with asymptotic speeds of order 0.2 – $0.3 c$. As this material expands and decompresses, it undergoes r-process nucleosynthesis, forming heavy nuclei. Radioactive decays heat the ejecta, causing it to radiate as a (red) kilonova.

The negative energy matter cannot escape. Most of the ingoing material falls immediately into the black hole. Some of the ingoing spiral has sufficient angular momentum to circle around the horizon, so that the inflow crashes into and shears against itself, leading to the formation of an initial *accretion disk*. (See Fig. 1.1, top.) The tidal disruption and appearance of an orbiting disk take place in of order a millisecond. The disk is initially strongly perturbed, with strong spiral waves. At the same time, the bound material that was initially outgoing begins to fall toward the black hole, and this *fallback material* incorporates itself into the disk. This *post-merger settling phase* lasts for tens of milliseconds, ending with a roughly axisymmetric black hole accretion system.

Shocks from the merger and settling quickly heat the gas in the disk to temperatures of a few to 10 MeV. The maximum density of the disk shortly after merger can be as high as $\sim 10^{12} \text{g cm}^{-3}$. At these densities and temperatures, the gas is efficiently cooled by neutrino emission. Neutrinos will carry energy away from the disk and also change the composition of the gas (the ratio of protons to neutrons), both on timescales of order 10 ms. The magnetic field inside the disk is amplified by several processes, including winding, Kelvin-Helmholtz vortices at shear layers, and the magnetorotational instability (MRI). The MRI drives turbulence, which provides a means of transporting angular momentum outward, causing the material in the inner disk to accrete into the black hole, the outermost material to move farther from the hole, and the disk as a whole to spread out. The cascade of energy to small scales also provides a heating source to offset the neutrino cooling.

The subsequent late post-merger evolution is driven by the interplay of neutrino and magnetic effects. The transport and heating effects of magnetoturbulence are often conceptualized and modeled as an effective viscosity, so that it is common to refer to its effects as “viscous” (e.g. “viscous winds”, “viscous timescale”), a custom we will follow, not without some reservation. To estimate the timescale of disk evolution, let us model the transport via a Shakura-Sunyaev alpha viscosity [29], in which case the effective kinematic viscosity is $\nu = \alpha_{\text{SS}} c_s H$, where c_s is the sound speed, H is the disk thickness, and α_{SS} is a dimensionless constant of order 10^{-2} –

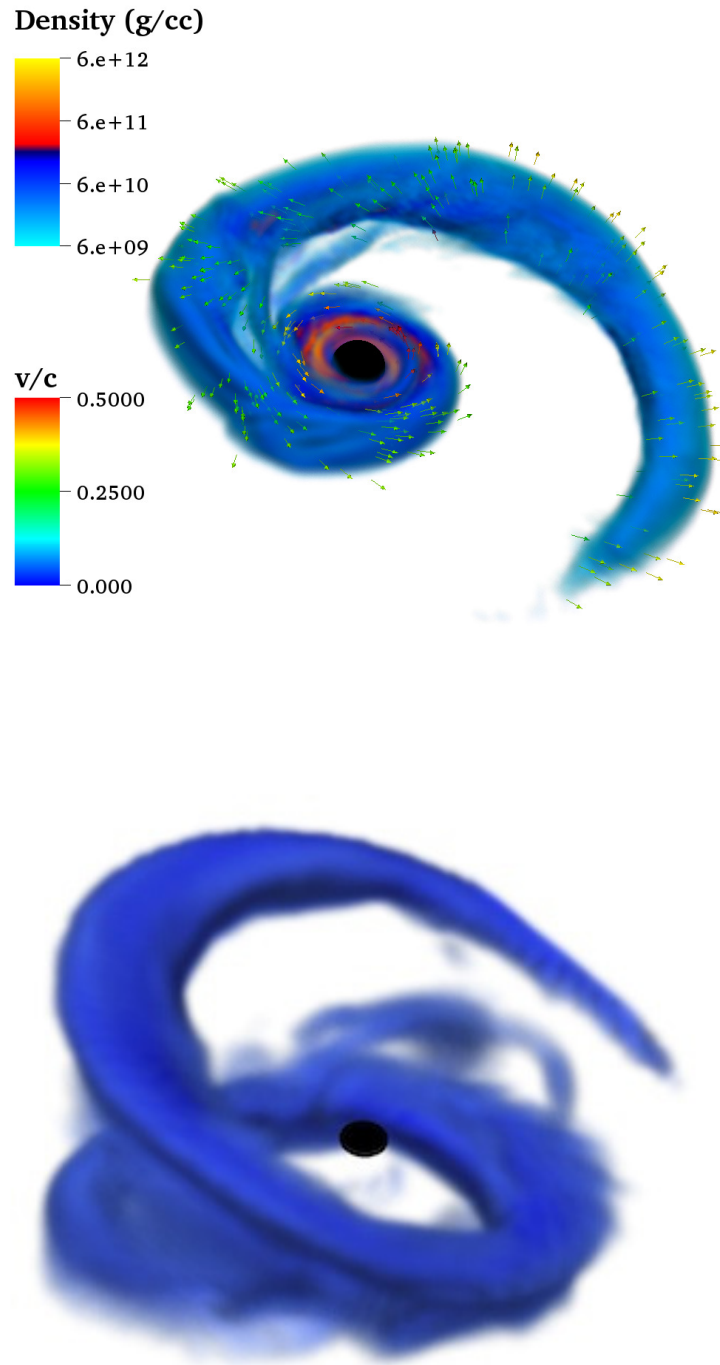


Fig. 1.1: Tidal disruption converts the neutron star into a spiral swath. **Top:** Incoming matter wraps around the black hole, crashes into itself, and forms a hot accretion disk. Color indicates density. (From Foucart *et al* [27].) **Bottom:** In this system with a massive black hole with black hole spin $\chi_{\text{BH}} = 0.9$ misaligned 40° from the orbital axis, there is orbital precession, and the stream avoids hitting itself. Shown is a density contour. (From Foucart *et al* [28].)

10^{-1} [30, 31]. Then the characteristic timescale for accretion and expansion is

$$\tau_{\text{visc}} \sim \alpha_{\text{SS}}^{-1} \Omega^{-1} (H/r)^{-2} \sim 10^2 \text{ ms} \quad (1.4)$$

where r is the distance from the black hole, and Ω is the Keplerian orbital velocity, and we have substituted values typical to a BHNS remnant disk.

For the first ~ 100 ms, neutrino luminosities are high (starting at $L_\nu \sim 10^{53}$ erg s^{-1}) and comparable to viscous heating, and the composition of the fluid is driven to an equilibrium of charged-current weak nuclear interactions. Perhaps a percent of the neutrino luminosity is deposited in the polar regions outside the disk through the annihilation of neutrinos and antineutrinos, heating matter there and possibly contributing to the initial formation of a jet. This is the *neutrino-cooled disk phase*. As the disk expands, its density and temperature drop, so that neutrino luminosity decreases, eventually becoming negligible, so that it no longer balances viscous heating. The disk is then said to be in an advective state. Viscous heating makes the disk thick and drives disk winds; these winds constitute a second source of unbound outflow, the *disk wind ejecta*, which contribute distinctly to the kilonova. This *advective disk phase* lasts longer than the previous phases as the disk depletes. One key goal of BHNS post-merger simulations is to characterize the disk wind outflows (their mass, composition, and speed) to determine the expected kilonova signals and nucleosynthesis output.

The most promising way to produce a relativistic jet, leading to a GRB, is through a poloidal magnetic field at the polar region near the horizon by the Blandford-Znajek mechanism [32]. Thus, a second key goal of magnetohydrodynamic (MHD) simulations of BHNS post-mergers has been to model the accumulation of magnetic flux on the horizon, the launching of the jet, and its eventual loss of power as the disk depletes, in order to enable comparisons with observed features of GRBs.

As the disk depletes, the accretion rate falls off with time according to a power law, which would suggest that accretion at a low level at least might continue for a long time. Eventually, after of order 100 seconds, energy from radioactive decays is sufficient to overcome the remnant disk's binding energy, which will quickly evaporate the disk and put an end to extended emission [33].

1.3 Binary parameter space and outcome fitting formulae

We expect the outcome of a BHNS merger to depend on Q , χ , and C . Let us consider how we expect these parameters to be distributed among actual BHNS binaries.

Unfortunately, these distributions are very uncertain, especially regarding the black hole properties. The black hole can be characterized by its mass M_{BH} and dimensionless spin χ . Observations of black holes in low-mass X-ray binaries show a narrow mass distribution at $7.8_{-1.2}^{+1.2} M_\odot$ [34]. In particular, there appears to be a mass gap between black hole and neutron star masses, with few black holes with mass less than $\approx 4.5 M_\odot$ [35]. Black holes in binary black holes detected by LIGO-Virgo have

broader distribution extending to higher masses [36]. The laws of classical physics permit black holes of any mass, including within the range of neutron star masses, but no known astrophysical process would produce black holes with masses below the neutron star maximum mass. (Primordial black holes, if they exist, might have low masses, though.) From gravitational wave signals, binary components are often identified as neutron stars or black holes by their mass, the subtle effects of finite size usually being undetectable. Some numerical simulations of BHNS mergers have considered very low $Q=1-1.2$ BHNS systems, in particular to see if they can be observationally distinguished from a binary neutron star system of equal component masses [37].

The distribution of inferred χ_{eff} in binary black holes peaks at +0.06, with a standard deviation of 0.12 [36]. It is, of course, possible that the black hole mass and spin distributions are different for BHNS binaries than they are in X-ray binaries and black hole-black hole binaries. Note that the black hole spin is a vector, and so it enlarges the dimension of our parameter space by three. Much numerical work has concentrated on the case of black hole spin aligned with (i.e. parallel to and in the same sense as) the orbital angular momentum because this turns out to be the most optimistic case for tidal disruption and electromagnetic signals.

What about neutron star masses and spins? Masses inferred from neutron stars in binaries range from about 1.2 to $2.0 M_{\odot}$ [38]. The mass distribution of galactic neutron stars in binary neutron star systems is rather narrowly peaked at $1.33 M_{\odot}$, but GW190425, the second detected binary neutron star merger signals, had a total mass of $3.4 M_{\odot}$, implying that higher mass neutron stars in these binaries are possible [39]. Furthermore, neutron stars in binaries with white dwarfs or main sequence stars have a wider distribution of masses, and peaked at a higher value, than neutron stars in NSNS systems [38]. We have seen that candidate BHNS gravitational wave signals infer a range of M_{NS} from 1.2 to $2.1 M_{\odot}$, with GW200115, the most confident case, having an inferred neutron star mass of around $1.5 M_{\odot}$.

Neutron stars do spin, but the fastest observed spins are in the millisecond range (millisecond pulsars), with a corresponding spin frequency (10^2 Hz) significantly smaller than the frequency of a BHNS system at merger (10^3 Hz). Furthermore, neutron stars with magnetic fields spin down and will have plenty of time to do so during the long inspiral. On the other hand, tidal forces and neutron star viscosity are too weak to spin up and tidally lock the neutron star before merger [40, 41]. Therefore, neutron stars are usually approximated as being irrotational (i.e. a curl-free velocity field) when constructing initial data for merger simulations. However, the effect of a non-trivial neutron star spin has been investigated in some simulations [42, 43], where it was found that the neutron star spin can affect the disk and dynamical ejecta masses.

It should be remembered that the total neutron star mass M_{NS} is distinct from the star's "rest" or "baryonic mass" M_{NS}^b . $M_{\text{NS}} < M_{\text{NS}}^b$ because of the negative gravitational potential energy, so $M_{\text{NS}}^b - M_{\text{NS}}$ is the star's binding energy.

Given the neutron star mass, and assuming slow spin ($\ll \text{ kHz}$), the radius of the neutron star, and hence the compaction, are determined by the properties of neutron star matter as codified in the equation of state, which supplies the pressure P as a

function of rest mass density ρ_0 . This function $P(\rho_0)$ is presumably unique—cold neutron stars have no free composition variables, unlike main sequence stars and white dwarfs. Unfortunately, this function is also unknown at high densities. One of the driving scientific interests in BHNS and NSNS binaries is to constrain it. This can be done by evolving systems with the same binary parameters (masses and spins) but different assumptions about the equation of state and determining how the observable outputs (gravitational wave and electromagnetic) depend on these assumptions. Thus, for the purposes of modeling, we must treat the equation of state as if it varied from one possible system to another. We will have much more to say about equations of state later (Section 1.4.2), so we defer this discussion until then. For the rest of this section, let us simply consider the compaction C to be a free parameter.

Thus, our 6D pre-merger binary parameter space has coordinates $(M_{\text{BH}}, M_{\text{NS}}, \chi, C)$. Can we define a parameter space of the merger outcome? We needn't be too concerned with the number of dimensions of this space; it is set by the number of outputs with which we are interested and does not affect the number of simulations we need to perform. Ideally, we would like to be able to express these output quantities as functions of the binary parameters. This can be done by using physical intuition to guess a form of the function, adding free parameters that can be fit using data from numerical simulations. The following outcome quantities have received the most attention.

A quantity whose dependence on binary parameters has received much attention is the post-merger baryonic mass, the material that “survives” by not falling immediately into the black hole M_{remnant}^b . Note that this “remnant” includes disk, fallback, and dynamical ejecta. Since the disk mass is not constant, but depletes due to accretion and wind, one must specify a time at which the mass is measured—10 ms after merger, for example. From the discussion in Section 1.2 above, we know that the presence of tidal disruption (and thus the possibility of a disk) depends on Q , C , and χ —the latter through its effect on R_{ISCO} . One might guess that the remnant mass depends on the same parameters. In fact, this works fairly well, as Foucart and collaborators have shown by positing $M_{\text{remnant}}^b/M_{\text{NS}}^b$ to be a simple function of the dimensionless numbers $\eta \equiv Q/(1+Q)^2$ (the “symmetric mass ratio”), C , and $R_{\text{ISCO}}(\chi)/M_{\text{BH}}$. They then used the results of available numerical simulations to fit the free parameters, and are able to achieve good a reasonably good fit [46, 44].

Fits also exist for the mass and speed of dynamical ejecta. Kawaguchi *et al* [45] carried out a large number of BHNS simulations, analyzed dynamical ejecta, and introduced fitting formulae. Their ejecta mass function involves C , Q , $R_{\text{ISCO}}/M_{\text{BH}}$, and the neutron star's specific binding energy $1 - M_{\text{NS}}/M_{\text{NS}}^b$. (See also [47] for a fit with better behavior for very compact neutron stars.) The ejecta mass is highest for $Q \approx 3$; it is small for very symmetric and very asymmetric binaries [48]. The ejecta velocity is adequately fit as a linear function of Q (with higher mass ratios producing faster ejecta).

Looking at the disk and dynamical ejecta masses in various regions of parameter space (see Fig. 1.2), we see that surviving matter tends to be disk-dominated at low mass ratio but ejecta-dominated at high mass ratios. Some fraction of the disk,

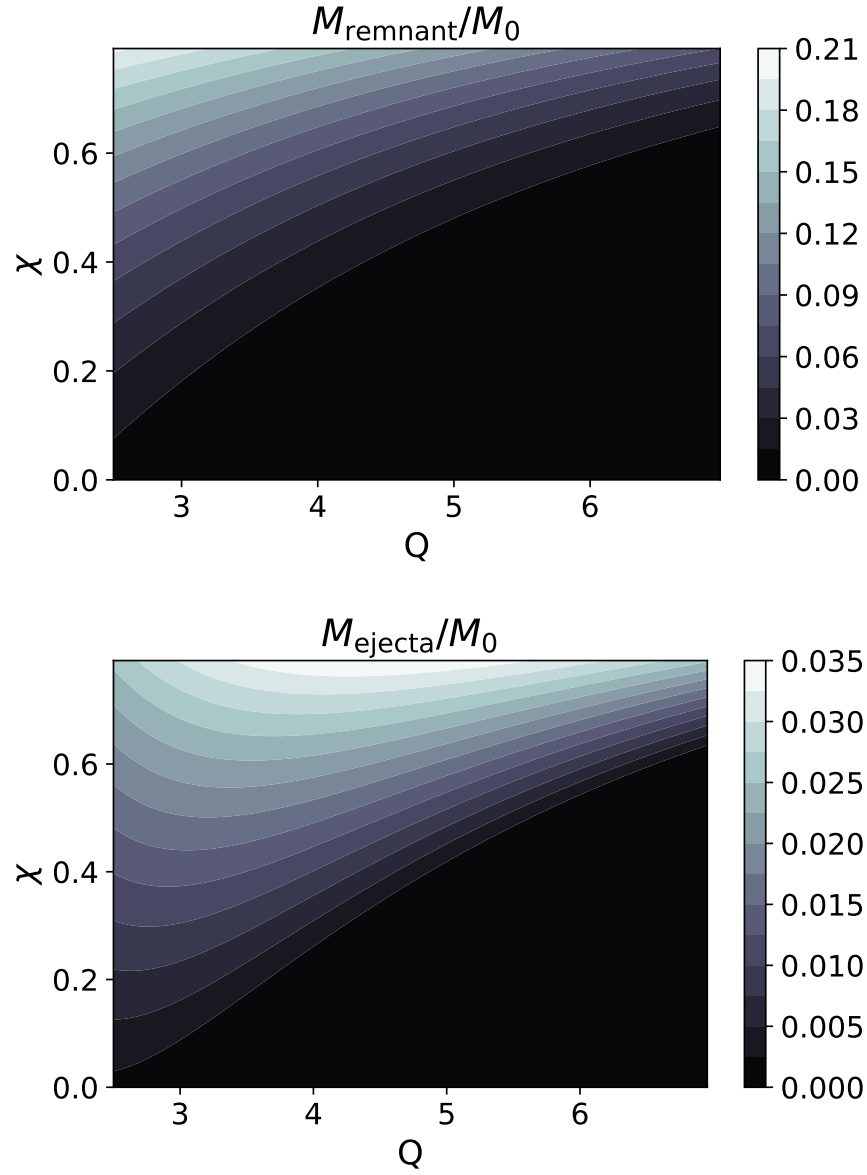


Fig. 1.2: Fraction of neutron star baryonic mass surviving in post-merger components as a function of mass ratio Q and dimensionless aligned black hole spin χ according to fitting formulae. Both plots assume a neutron star with compaction 0.161 and specific binding energy 0.094. **Top:** remnant mass after 10 ms according to the formula of Foucart *et al* [44]. **Bottom:** dynamical ejecta mass according to the formula of Kawaguchi *et al* [45].

perhaps between 5% and 30% of its mass, will be ejected in winds (see Section 1.9 below). Disk outflow mass will then presumably also dominate dynamical ejecta mass only for very low $Q \lesssim 3$. For some range of parameters, the two components will both be important, and for high Q (and high prograde spin, so that the binary is disrupting), ejecta will mostly be dynamical. This is important, because we will see that the two ejecta components have very different properties.

Attempts have also been made to fit outcomes related to the spacetime. Pannarale fit for the post-merger black hole’s mass and spin [49, 50]. (See also [51].) The gravitational wave cutoff frequency could then be fit as a function of these remnant properties [52, 53]. We will return to modeling the gravitational waveform in Section 1.5.

1.4 Ingredients of a numerical simulation

1.4.1 Gravity, plus a bit of history

1.4.1.1 Newtonian

BHNS binaries are strong gravity systems, but for decades numerical relativists were unable to stably evolve dynamical black hole spacetimes (although they could make progress on binary neutron stars [54]), so the early BHNS simulations were carried out using Newtonian physics, with the neutron star represented as an ideal fluid and the black hole as a point mass [55, 56, 57, 58, 59]. A key question was what happens when R_{tidal} is reached and mass transfer begins. These simulations found cases in which mass transfer once begun leads to the complete disruption of the neutron star but also cases where mass loss causes the neutron star to retreat into its Roche lobe so that the flow of matter off the neutron star stops and a neutron core survives to another episode of mass transfer. They found soft equations of state to favor unstable mass transfer, stiff equations of state to favor episodic mass transfer. In fact this turned out to be an artifact of Newtonian gravity; relativistic mass transfer is more unstable.

In fact, one can get qualitatively correct results, for which tidal disruption happens in one pass even for stiff realistic equations of state, by replacing the Newtonian point mass potential with “pseudo-Newtonian potentials” designed to mimic certain features of black hole orbital dynamics [60, 61]. The most common of these are the Paczynski-Wiita potential [62] (for modeling nonspinning black holes) and the Artemova *et al* potential [63] (for modeling spinning black holes).

It is worth pausing to gain a sense of these techniques because much of the work on late-time accretion and disk wind ejecta to be discussed later uses Newtonian physics and pseudo-Newtonian potentials. The Paczynski-Wiita potential is just $\Phi(r) = -M_{\text{BH}}/(r - 2M_{\text{BH}})$. The simple addition of the extra term in the denom-

inator reproduces the innermost stable circular orbit location of a Schwarzschild black hole (for Schwarzschild radial coordinate).

1.4.1.2 Relativistic

It is beyond the scope of this chapter to explain the techniques used to stably evolve spacetime metrics (for a book-length treatment, see [64]), but perhaps we can briefly convey the flavor of it. To handle gravity relativistically, one must calculate the spacetime metric $g_{\mu\nu}$. The metric provides not only what our Newtonian intuition regards as gravitational effects but also automatically supplies the properties of the black hole and of the gravitational waves, because these three are all just different aspects of the spacetime curvature. The Einstein field equations are nonlinear second-order partial differential equations for $g_{\mu\nu}$. The field equations come in two types: *evolution* equations, which supply the time derivatives that tell how the metric changes from one time slice to the next, and *constraint* equations, which restrict how the fields must relate at each time. This is entirely analogous to the split in Maxwell's equations, e.g. Faraday's law $\partial_t \mathbf{B} = -\nabla \times \mathbf{E}$ is an evolution equation while Gauss's Law $\nabla \cdot \mathbf{E} = 4\pi\rho$ is a constraint which must be satisfied at each time. (Analytically, if the constraints are satisfied at one slice of time, the evolution equations will keep them satisfied at later times, as with Maxwell's equations. Whether numerical-error induced constraint violations remain small depends on one's formulation of Einstein's equations.) The numerical relativist must supplement Einstein's equations with a third set of equations, the *gauge* conditions, which determine the choice of coordinates, e.g. how spacetime is to be sliced into space and time.

A key part of any numerical relativity calculation is the construction of appropriate initial data. For a BHNS simulation, this must correspond to a black hole and a neutron star in circular orbit. Numerical costs (above all the number of timesteps involved) motivate us to create binaries in the late inspiral stage, no more than roughly a dozen orbits before merger. To be a time slice of a solution of Einstein's equations, the constraint equations must be satisfied at this $t = 0$ slice. This amounts to four elliptic partial differential equations that must be solved.

In addition, one wants to impose the conditions that the star is in equilibrium and the binary is in circular orbit, which will not be true for just any choice of density distribution, orbital rotation rate, and (constraint satisfying) metric. It is impossible to impose an exact, consistent circular orbit symmetry on the spacetime, impossible because a BHNS orbiting in perfect circles forever is not a solution to Einstein's equations—actually, there must be gravitational radiation and inspiral. What is actually done, in what is called the extended conformal thin sandwich (XCTS) formulation, is to freely choose some metric variables and then use the constraints and assumed circular orbit to solve for the remaining five. For example, one factors the three-metric as $\gamma_{ij} = \Psi^4 \tilde{\gamma}_{ij}$, chooses $\tilde{\gamma}_{ij}$, e.g. to be flat or to resemble a single black hole space, and solves for Ψ with a constraint equation. Making slightly wrong assumptions makes the problem tractable, but it comes at a cost. An incorrect $\tilde{\gamma}_{ij}$ means unphysical (“junk”) gravitational radiation in the initial data. Ignoring inspi-

ral produces slightly eccentric orbits (which can be reduced by adding some initial inspiral [65]).

Equilibrium must also be imposed on the fluid. The Euler equation can be integrated to give an algebraic condition (with integration constant), the relativistic generalization of the Bernoulli integral. This turns out to be an equation for $h\Gamma$, where h is the specific enthalpy, and Γ is the Lorentz factor. Thus, given the fluid velocity, equilibrium gives h and thus (via the equation of state) ρ_0 . The condition that the star is non-spinning is translated as the condition that the flow is irrotational. Recall that in Newtonian physics, this means $\nabla \times \mathbf{v} = \mathbf{0}$ so that $\mathbf{v} \equiv \nabla\phi$, and the relativistic version is similar. An elliptic equation for the velocity potential ϕ is supplied by the continuity equation.

To the extent that the inspiral timescale is much longer than the orbital timescale, one can think of the binary as simply evolving from one of these quasi-equilibrium circular orbit states to another. One can, then, track the inspiral evolution of a single binary by creating a sequence of these equilibria at different separations, holding fixed quantities like the neutron star baryonic mass and black hole irreducible mass (expected to be nearly conserved since little of the gravitational wave energy is swallowed by the black hole.) At smaller separations, the orbital angular velocity Ω increases; in fact, Ω is a better parameter along the sequence than coordinate separation, because it can be calculated in a coordinate-invariant way. As the binary inspirals to higher Ω , the total energy (ADM mass) of the binary goes down, with the reduction presumably accounted for by gravitational wave emission. Before numerical relativity evolutions were possible, these sequences provided our best understanding of the late inspiral [66, 67, 68]. The most interesting question was how the quasi-equilibrium sequences end. The ISCO of a sequence is where the binary's energy as a function of Ω reaches a minimum. The onset of tidal mass transfer is indicated by the formation of a cusp shape on the stellar surface. Unfortunately, this final and most interesting part of the sequence is precisely where inspiral is becoming rapid and the quasi-equilibrium assumption certainly breaks down. Thus, we are compelled to do full evolutions to model the end of the inspiral credibly.

For further reading on initial data construction, see [69].

Numerical relativity experienced a breakthrough in its ability to stably evolve binaries with black holes in 2005. (For a review of numerical relativity centering on this breakthrough and the work it enabled, see [70].) The next year, Loffler *et al* [71] simulated a BHNS head-on collision, and Shibata and Uryu carried out the first fully relativistic simulations of BHNS merger starting from roughly circular orbit [72]. This was quickly followed by other groups [73, 74, 75].

1.4.2 Equation of state

BHNS simulations must model matter in a wide range of densities and temperatures. The high density matter inside neutron stars and the low density matter in disks and outflows each present their own challenges.

In general, the gas will be composed of a combination of photons, leptons, and baryons, with the baryons divided into free protons (p), free neutrons (n), and many different species of nuclei. At temperatures above about 0.5 MeV, we can invoke the wonderful simplification of *nuclear statistical equilibrium* (NSE). That is, strong nuclear reactions proceed so quickly that the abundances of each nuclide (including free nucleons) quickly come to their equilibrium values, and this equilibrium is maintained as fluid elements evolve. Then the composition of each isotope is fixed by a network of Saha-like equations, and the state of the fluid can be described by only three variables: the number density n (actually, the numerical relativity community prefers the equivalent number, the baryonic density ρ_0 , which is just n multiplied by a standard baryonic mass), the temperature T , and the fraction of baryons that are protons $Y_e \equiv n_p/(n_p + n_n)$. The latter, Y_e , is sometimes called the reduced electron fraction and is what is being referred to when numerical relativists speak of the “composition” of our outflows. Note that Y_e of a fluid element can only change because of charged-current weak interactions (which can change protons to neutrons, and vice versa), which also create and absorb neutrinos. The timescale for these weak interactions to come to equilibrium is not always small compared to evolution timescales, so Y_e must be evolved. The equation of state thus provides pressure P and specific internal energy ε as functions of (ρ_0, T, Y_e) . Nuclear physics equation of state models provide these to numerical relativity codes in tabulated form.

Before merger, the neutron star matter is very degenerate, so one can take $T = 0$. Furthermore, the neutron star will have had time to settle to equilibrium to weak interactions (“neutrinoless beta-equilibrium”). The latter equilibrium condition ($\mu_p + \mu_{e^-} - \mu_n = \mu_{\nu_e} = 0$, where μ_X , denoting the chemical potential of particle X , is a function of ρ_0 , T , and Y_e given by the equation of state) amounts to a condition on Y_e , so the equation of state becomes one-dimensional: $\varepsilon = \varepsilon(\rho_0)$, $P = \rho_0^2 d\varepsilon/d\rho_0$.

This 1D equation of state is all that is needed for initial data and, because most of the gravitational waveform comes from the inspiral, it is sufficient for most gravitational wave studies. Systematic studies of the effect of equation of state have been carried out assuming the piecewise polytrope family of equations of state. Here, one divides the density into intervals and takes the pressure in each interval to be a simple power law of the density. For example, in interval i covering densities between $\rho_{0,i-1}$ and $\rho_{0,i}$, one has $p(\rho_0) = \kappa_i \rho_0^{\Gamma_i}$, where κ_i and Γ_i are constants. For chosen $\rho_{0,i}$, Γ_i , and κ_0 , one can infer the other κ_i by requiring continuity in $p(\rho_0)$. The range of realistic behavior can be captured with three free parameters [76]. One downside to piecewise polytropes is that they are not smooth at the boundaries of intervals, meaning the sound speed is discontinuous. There is a simple generalization to the equation of state family that fixes this [77].

An alternative flexible but smooth equation of state family is available using “spectral” equations of state [78, 79]. Here one takes the independent variable to be $x \equiv \ln(\rho_0/\rho_0^{\text{ref}})$ for some reference density ρ_0^{ref} . The adiabatic index $\Gamma(x) \equiv d \ln(P)/dx$ is specified as a sum of basis functions (hence “spectral”), and then $P(x)$

and $\varepsilon(x)$ can be recovered by appropriate integrals. In fact, the simple choice of a polynomial $\Gamma(x) = \sum_{n=0}^N a_n x^n$ suffices.

After merger, the densities in disks and outflows are low enough that nuclear forces are unimportant (except in the sense of holding nuclei together), and the equation of state is just a combination of classical ideal cases for free nucleons and nuclei, ideal Fermi gases for electrons/positrons, and photon radiation. As the disk expands, the NSE equilibrium changes from free nucleons to alpha particles and heavy nuclei. This recombination of nucleons releases binding energy, providing a source of thermal energy that is important for disk winds. Note that this is a reversible process; it does not generate entropy. Conservative MHD codes do not need to add a “heating” term, since the negative binding energy automatically means more thermal energy at a given total energy.

Simulations that follow disks and outflows for second timescales run into the problem of temperatures $\ll 0.5$ MeV, which makes the continued assumption of NSE dubious. In particular, heating from r-process nucleosynthesis might on second timescales provide a significant source of thermal pressure, and such an effect cannot be captured with an NSE code. Unfortunately, the only adequate solution of dropping NSE and evolving isotope abundances via nuclear reaction rates would mean an explosion of evolution variables describing the composition of the fluid. Instead, a few studies have tried to add phenomenological heating terms to estimate the effects of this heating on outflows and fallback [80, 81, 82]. More recently, the necessary step of dropping NSE has been undertaken with simulations with a nuclear reaction network evolving nuclide abundances coupled to 2D ray-by-ray hydrodynamic evolution of the outflow [83].

1.4.3 Neutrino transport

After merger, the surviving orbital material heats to $T \sim \text{MeV}$, and neutrinos are copiously produced by weak nuclear interactions, including particularly the charged-current reactions, which alter Y_e and produce electron-flavor neutrinos and antineutrinos



and the electron-positron pair annihilations, which produce neutrinos of all flavors i



Immediately post-merger, neutrino luminosities reach $L_\nu \sim 10^{53} - 10^{54} \text{ erg s}^{-1}$. The thermal energy of the newborn disk is $E_T \sim 10^{52} \text{ erg}$, suggesting a thermal timescale of $\tau_{\text{th}} \sim 10 - 100 \text{ ms}$ [84].

Electron-type neutrinos can also be absorbed by the reverse of the processes of Eq. 1.5 and Eq. 1.6. In addition, neutrinos of all flavors scatter off of free nucleons and nuclei. There will thus be, for neutrino species i , an opacity for absorption $\kappa_{i,a}$, an opacity for scattering $\kappa_{i,s}$, and a total opacity $\kappa_i = \kappa_{i,a} + \kappa_{i,s}$. (As with photon transport, κ_i is neutrino energy-dependent, and absorption and scattering can have somewhat different effects—details which are important in a radiation transport code but which will be ignored henceforth in this overview.) The associated mean free path is $\ell_i = 1/\kappa_i$ [or $1/(\kappa_i\rho_0)$, depending on how one defines κ_i]. How important will these scatterings and absorptions be in a post-merger disk? To answer that, one can compute the optical depth, which for a disk of height H will be $\tau_i \sim H/\ell_i$. If $\tau_i \ll 1$, the disk is optically thin, i.e. transparent, and opacity is unimportant. Emitted neutrinos travel outward from their emission sites along almost null geodesics. If $\tau_i \gg 1$, the disk is optically thick; neutrinos are trapped, come to (Fermi-Dirac) equilibrium, escape more slowly by random walk / radiative diffusion, and can even be advected with fluid into the black hole. For BHNS disks, τ_i is at most of order ~ 10 , but after a viscous timescale of disk depletion will almost certainly be optically thin.

Because τ_i ranges from low to high, evolving the neutrino fields is difficult. Each neutrino species is described by a distribution function (the density in phase space) $f(\mathbf{x}, \mathbf{p})$. The evolution equation of f , the Boltzmann transport equation, is simple, but the fact that it is 6-dimensional makes it expensive even to store a reasonable numerical representation of it.

Many of the BHNS simulations that include neutrino effects use *neutrino leakage*, i.e. they do not evolve the neutrino fields at all, but only add a cooling term in the fluid evolution, as well as a source term for Y_e to account for lepton number changes from Eq. 1.5 and Eq. 1.6. For $\tau_i \ll 1$, one can get these from the local emission rates; for higher τ_i , one must approximate, at least to order of magnitude, the effect of diffusion. These methods decently capture neutrino cooling and were used for the earliest studies of BHNS mergers that incorporated weak interactions [58, 60, 84, 27, 85], but they have the serious drawback that neutrinos emitted in one part of the grid cannot be absorbed in another part.

A more sophisticated way to model neutrinos is provided by an *M1 moment closure scheme* [86, 87], which rather than evolving all of f only involves its lowest two moments: the neutrino energy and momentum densities. Most codes integrate the specific neutrino energy and momentum density over neutrino energies and evolve only the energy-integrated densities. Such transport schemes are called “grey”. The evolution equation of each neutrino moment involves the next higher moment, so in order to obtain a closed, finite set of equations, one must assume the form of the first moment not evolved, i.e. one must provide a “closure condition”. M1 does capture neutrino absorption, and it has been used in two studies of BHNS mergers [88, 89], which found that neutrino irradiation of dynamical ejecta does not significantly affect its composition, but the disk Y_e profile is noticeably different than predicted by leakage. Although a great improvement upon leakage, grey M1 remains imperfect, both because of imperfection in the closure condition and the sacrifice of spectral information.

Recently, some numerical relativity codes have evolved the full Boltzmann transport equation for the full neutrino distributions using *Monte Carlo* methods [90, 91]. Monte Carlo transport coupled to MHD was used to evolve a post-merger-like disk with the code `vbhlight` [92]. The disk had an initial optical depth of ~ 10 , so neutrino absorption is able to significantly affect the Y_e distribution of the disk and its outflows.

In addition to carrying energy, emitted neutrinos carry their momentum away with them, meaning neutrinos can provide a source of physical viscosity. Under some conditions, this viscosity could significantly slow the growth of the MRI [93]. If the MRI is suppressed, momentum transport in the disk will be greatly slowed, since the neutrino viscosity itself would be much weaker than the turbulent effective viscosity that would otherwise be present. Guilet *et al* [94] have made a careful study of the effect of neutrino momentum transport on the MRI. They find that neutrino effects behave like a viscosity if the neutrino mean free path ℓ is much smaller than the wavelength of the fastest growing MRI mode: $\ell < \lambda_{\text{MRI}}$. If $\ell > \lambda_{\text{MRI}}$, neutrinos act as a drag force. For realistic (i.e. not-magnetar) initial fields, early post-merger λ_{MRI} is small enough that neutrinos will act as a drag. Simulations indicate that the drag’s damping timescale is at least initially much longer than the orbital timescale on which the MRI grows [88, 95], meaning neutrinos probably will not prevent a phase of exponential field growth.

Adequate treatment of neutrino physics remains a serious challenge for BHNS simulations. Even the most sophisticated of the above schemes ignore neutrino flavor oscillations, which might affect outflow compositions [96, 97]. For a review of neutrino transport methods in numerical relativity, see [98].

1.5 Gravitational waves

The inspiral gravitational waveform of a BHNS binary is, like the waveform from a binary black hole (BHBH) or a NSNS binary, well described by the waveform expected for a binary of two point masses. However, the fact that the neutron star is an extended object does leave a small imprint on the waveform. The gravity of the black hole tidally deforms the neutron star, giving it a quadrupole moment which affects the binding energy E and contributes to the gravitational wave luminosity L_{GW} . To lowest post-Newtonian order, the effect of tides on the gravitational wave phase depends only on one numerical property of the neutron star: its tidal deformability Λ , the ratio of the induced quadrupole moment of the star to the perturbing tidal gravitational field, in this case from the black hole [99]. This number Λ is strongly dependent on the compaction of the neutron star; it is, in fact proportional to R_{NS}^5 . Thus, if this phase drift could be detected, it would provide a way of estimating the neutron star radius. Unfortunately, the tidal effect is smaller at higher Q , so BHNS systems are less promising for this sort of measurement than NSNS systems.

The effect of the end of the inspiral on the gravitational wave is dramatic, although unfortunately in the poorly accessible kHz range. The best way to under-

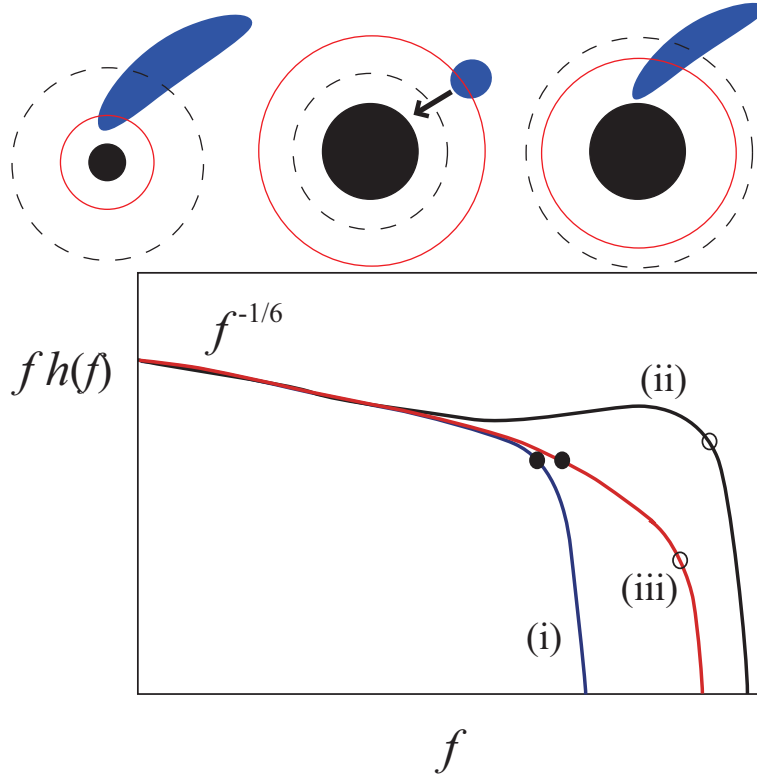


Fig. 1.3: Schematic pictures of three different merger types and their corresponding gravitational wave spectra. In the top pictures, the solid circle is the ISCO location, the dashed circle the location of tidal disruption. The types are (i) disruption with disrupted star larger than the black hole, (ii) plunge, and (iii) disruption with disrupted star smaller than the black hole. Reprinted figure with permission from Kyutoku, Okawa, and Shibata, *Phys. Rev. D* **84** 064018 (2011) [51]. Copyright 2011 by the American Physical Society.

stand the BHNS waveform is to compare it to a BHBH waveform. BHBH waveforms have three parts: (1) the inspiral waveform, during which the amplitude and frequency ramp up, (2) the merger waveform, at which the waveform amplitude peaks, and (3) the ringdown, a damped oscillation waveform representing the decaying perturbed modes of the settling black hole. Recall that BHNS inspiral may end, and merger may commence, in one of three ways: plunge ($R_{\text{ISCO}} > R_{\text{tidal}}$), tidal disruption ($R_{\text{ISCO}} < R_{\text{tidal}}$), or both together ($R_{\text{ISCO}} \approx R_{\text{tidal}}$). Using numerical relativity simulations for a range of Q , Shibata *et al.* [100] found that these three types of inspiral termination correspond to three types of BHNS merger gravitational waveforms, as illustrated in Figure 1.3.

Systems in which the neutron star plunges into the black hole before significant mass transfer have waveforms very similar to BHBH waveforms, with inspiral, merger, and ringdown. (Indeed, the waveform is almost identical to that of a BHBH system with the same component masses [101].)

If tidal disruption happens well outside R_{ISCO} , the waveform cuts off during the inspiral segment, and the wave amplitude decreases quickly as the disrupted neutron star spreads out and the binary’s quadrupole moment drops. The matter falls through a broad, roughly axisymmetric region of the black hole and does not excite strong, coherent quasi-normal modes on the black hole, so in this case there is no ringdown waveform. One would guess that the frequency at which the waveform drops would be given by f_{cut} (cf. Section 1.2), the frequency corresponding to where mass transfer begins. Actually, the true cutoff frequency is higher, at the frequency at which the neutron star is fully tidally disrupted. The distinction has a significant effect on the dependence of the gravitational wave cutoff on the neutron star compaction [102, 51, 23]. More compact neutron stars not only begin mass transfer closer to their black hole; they also survive mass transfer longer.

There remains the intermediate case in which plunge and tidal disruption happen together. The type of waveform in this case depends on the black hole mass. For $Q \lesssim 3$, one sees an intermediate waveform type with inspiral and merger but very weak ringdown component. For higher Q with tidal disruption near the ISCO, which requires high prograde black hole spin, the ringdown component remains present. The reason is that although the neutron star is spread out by tidal disruption, if the black hole horizon is bigger than the original neutron star, the disrupted star still flows through a localized region of the horizon.

Since R_{tidal} depends on C , the waveform cutoff in disrupting cases has information about the neutron star and its equation of state. The information contained in the cutoff frequency in fact turns out to be nearly equivalent to Λ , presumably because both Λ and C depend (for known M_{NS}) mostly on R_{NS} . An ambitious numerical exploration of the BHNS parameter space was carried out with the SACRA code by Lackey *et al* [103]: 134 simulations varying mass ratio, (aligned) black hole spin, and neutron star equation of state. To explore possibilities of the equation of state, a piecewise polytrope family with two free parameters was used. Although their equation of state space was 2D, a Fisher matrix analysis confirms that waveforms allow one best to measure one equation of state parameter, the tidal deformability.

It would be impossible to produce numerical relativity waveforms for every set of binary parameters that gravitational wave observatories might need as templates for detection and parameter estimation. Instead, the hope is to use waveforms from a smaller number of BHNS simulations to calibrate some simpler waveform model for which cases can be generated quickly. Thus, finite-size corrections have been added to the phenomenological (“Phenom”) and effective one-body (“EOB”) families of binary inspiral-merger-waveforms. The Phenom BHNS waveforms [103, 52, 104] were calibrated to the 134 SACRA waveforms. The EOB BHNS waveform models [105] were calibrated to SACRA and SpEC numerical waveforms.

One way to test the adequacy of these models for LIGO-Virgo purposes is to insert numerical relativity waveforms into LIGO noise and see if the signals can be

detected and the binary and equation of state parameters correctly extracted using the model waveforms as templates. Waveform models are considered good enough if the systematic errors from model inaccuracies are lower than the expected statistical errors (given whatever signal to noise ratio one is hoping for). See [106, 107] for checks of this sort.

1.6 Magnetospheres

Neutron stars observed as pulsars have magnetic fields that extend outside the neutron star surface into a magnetosphere region. In a BHNS binary, this neutron star magnetosphere could extend to and begin interacting with the black hole prior to merger. Electromagnetic signals from this magnetosphere interaction are interesting for two reasons. First of all, the signal could actually precede the merger and so perhaps appear shortly before a GRB. Second, this magnetosphere interaction and accompanying signal could still occur even for nondisrupting BHNS binaries (recall: $R_{\text{ISCO}} > R_{\text{tidal}}$), which otherwise seem to be such duds, electromagnetically speaking.

In the neutron star magnetosphere, the energy density and stresses of the electromagnetic field dominate over that of the fluid, i.e. $T_{\text{EM}}^{\mu\nu} \gg T_{\text{fluid}}^{\mu\nu}$; in this limit, the fluid’s pressure and even its inertia can be ignored [108]. Energy-momentum conservation then gives

$$\begin{aligned} 0 &= \nabla_{\nu}(T_{\text{EM}}^{\mu\nu} + T_{\text{fluid}}^{\mu\nu}) = \nabla_{\nu}(T_{\text{EM}}^{\mu\nu}) = F^{\mu\nu} \mathcal{J}_{\nu} & (1.8) \\ \mathbf{0} &= \rho_e \mathbf{E} + \mathbf{J} \times \mathbf{B} & (1.9) \end{aligned}$$

where $F^{\mu\nu}$ is the Faraday tensor, \mathcal{J}_{ν} the 4-current, ρ_e the charge density, and \mathbf{J} the 3-current. This is called the “force free limit” because the above stress-energy condition is really a statement that momentum doesn’t get transferred from the electromagnetic field to the fluid (i.e. no force on it). It should be emphasized that, even though $T_{\text{fluid}}^{\mu\nu}$ is negligible, the force-free limit is very different from the vacuum Maxwell limit. The fluid contributes not inertia but free charges which provide conductivity. Notice from Eq. 1.9 that $\mathbf{E} \cdot \mathbf{B} = 0$. That is, there can be no electric potential difference along a magnetic field line; magnetic field lines are like *wires*.

Force-free evolutions often lead to the formation of regions in which the force-free approximation (and ideal MHD itself) breaks down. This will happen at current sheets, where \mathbf{J} becomes large and the force-free condition $B^2 > E^2$ breaks down. Inside current sheets, the effects of resistivity (ignored by ideal MHD) become important, and magnetic field lines reconnect, releasing energy and producing isolated magnetic field loop regions (plasmoids).

The same unipolar inductor model that has been used to explain the Blandford-Znajek effect was used to predict electromagnetic energy release from BHNS magnetosphere interaction [110]. In the original Faraday disk, a spinning conducting disk threaded by a magnetic field has an electric field (by the MHD condition

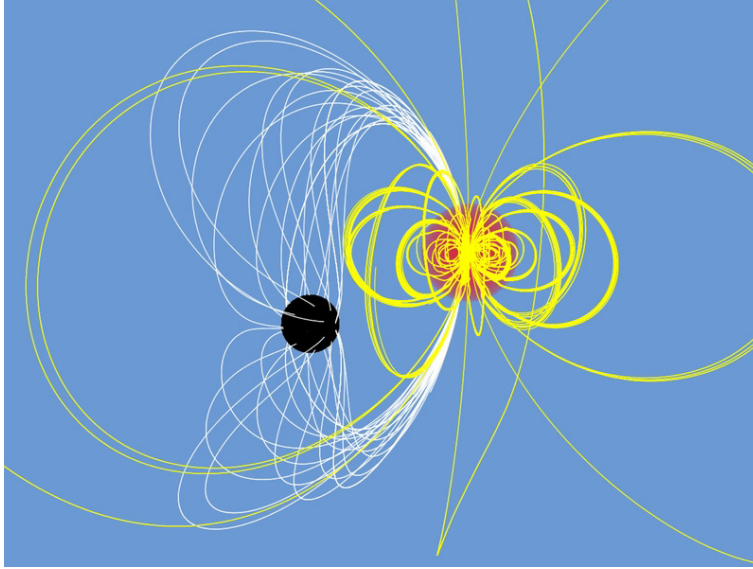


Fig. 1.4: Magnetic field lines from a neutron star magnetosphere interacting with a black hole before merger. Reprinted figure with permission from Paschalidis, Etienne, and Shapiro, *Phys. Rev. D* **88**, 021504 (2013) [109]. Copyright 2013 by the American Physical Society.

$\mathbf{E} = \mathbf{B} \times \mathbf{v}$) and so a potential difference; by touching the disk at different points with wires, the disk can be used as a battery. In the Blandford-Znajek mechanism, the black hole horizon and magnetic field lines play analogous roles. A similar unipolar inductor model of a BHNS system would predict an energy-releasing black hole battery circuit driven by the orbital motion of field lines at the horizon.

This has been modeled in numerical relativity by Paschalidis *et al* [109] using an ideal MHD code able to extend to the force-free limit [111] and by East *et al* [112] and Most *et al* [113] using resistive MHD codes whose chosen form of Ohm's law recovers the force-free limit in the appropriate regime [114]. A snapshot from one such simulations showing magnetic field lines from the neutron star magnetosphere under the influence of the black hole is shown in Figure 1.4. All of these studies report the electromagnetic energy outflow as a component of energy output. This can be calculated from the Poynting flux through an arbitrary distant sphere. One can also compute energy drained from the magnetic field via reconnection in current sheets [115].

The unipolar inductor model is found to estimate well the Poynting power output near the time of merger. In the magnetosphere of an isolated pulsar with spin angular frequency Ω , a crucial role is played by the light cylinder, the cylindrical radius $\varpi \approx c/\Omega$ at which the magnetosphere would have to orbit at the speed of light to spin at the same rate as the star, where one sees a switch from corotating closed field

lines inside to open field lines and a current sheet. Similarly, in the BHNS, there is an orbital light cylinder at $\varpi \approx c/\Omega$ with Ω the orbital angular frequency, and the black hole twisting field lines close to this cylinder plays an important role in the energy release. Energy is released both by reconnection heating and by outgoing Poynting flux. The resulting radiation might be observed as a fast radio burst or X-rays.

1.7 Disk formation and structure

Relativistic simulations confirm that tidal disruption occurs in a single pass, even for stiff realistic equations of state [116]. Episodic mass transfer, as well as other interesting dynamics, *is* possible in general relativity for the merger of *eccentric* BHNS binaries [117]. Relativistic simulations are also the most reliable for studying the effect of black hole spin. Aligned prograde spin can make what would have been nondisrupting binaries disrupting and leads to more massive remnant disks [118, 51, 119], retrograde spin has the opposite effect, and misaligned spins have intermediate effect. This influence on disk mass is reproduced by Foucart’s fitting formulae [46, 44] through the effect of black hole spin on R_{ISCO} . For high mass ratios $Q \gtrsim 5$, corresponding to what are likely the most common black hole masses, disruption and massive disk formation are only possible for high ($\chi_{\text{BH}} \gtrsim 0.7$) prograde spin [120], suggesting the depressing (to multimessenger astronomers and MHD numericists) likelihood that most BHNS mergers in nature are non-disrupting. High Q BHNS binaries that do disrupt have a larger fraction of the surviving matter outside the black hole in dynamical ejecta as opposed to disk [28, 121].

If the black hole spin is misaligned with the orbit, then there are additional effects of the spin [122, 28, 123]. Spin-orbit coupling leads to orbital precession—the neutron star and black hole “bob” above and below the initial orbital plane. For high misalignment angles ($\gtrsim 40^\circ$) and high black hole spin, there can be notable differences in the post-merger state. If the neutron star disrupts, the swath of matter is not restricted to one plane, so it can avoid hitting itself, at least for a time, as it wraps around the black hole, delaying the formation of a disk. (See bottom panel on Fig 1.1.) Disks from significantly misaligned systems are themselves misaligned, orbiting in a plane inclined with respect to the equator defined by the black hole’s spin, although this inclination angle decreases on a timescale of tens of milliseconds. Disk-black hole spin misalignment can also lead to precession of the jet, which could produce a periodicity in an observed GRB signal as the angle between direction of jet and direction to observer oscillates. Since binary neutron star mergers do not seem to have a means of producing such misalignments, this precession-induced GRB periodicity has been suggested as a way of distinguishing GRBs from BHNS mergers [124].

In the outgoing tidal tail, some matter will be unbound and some bound. The unbound matter contributes to outflows discussed below in Section 1.9. The bound material eventually falls back onto the central black hole plus disk. Treating the

bound outflow as following highly eccentric Keplerian orbits, one can compute the fallback time, and from that the mass inflow rate $\dot{M}_{\text{fallback}}$. This is found to follow a $t^{-5/3}$ power law [125, 75, 85]. This is explained as follows [126, 127, 128]. The specific orbital energy e is related to the semimajor axis a and the period t by $e \sim a^{-1} \sim t^{-2/3}$. Then the mass falling back in time interval $dt = dP$ is $dM = (dM/de)(de/dt)dt \sim t^{-5/3}(dM/de)dt$. If the ejecta/fallback mass distribution is nonzero at $e = 0$, then zooming into a narrow enough range of e near zero (corresponding to very late fallback times), the distribution will look flat, and the fallback rate will asymptote to $\dot{M} \sim t^{-5/3}$. In fact, dM/de of bound ejecta is pretty flat, so most of the fallback obeys the $t^{-5/3}$ rate [23].

In the first tens of milliseconds, fallback onto the disk can exceed accretion into the black hole and significantly perturb and grow the disk. The power law falloff in $\dot{M}_{\text{fallback}}$ would suggest that fallback can persist till late times, later than the (viscous timescale) lifetime of the postmerger disk, so that fallback has been considered as a source of late-time (\sim hour) extended emission from some GRBs. However, two considerations alter the expectation of an uninterrupted power law evolution of $\dot{M}_{\text{fallback}}$. First, the accretion disk itself generates outgoing winds which would be expected to interfere with fallback flows. Indeed, a study by Fernández *et al* [129] on the interplay between disk winds and dynamical ejecta shows that, for a $Q \approx 7$ merger, disk winds can overcome and suppress fallback for times after about 100 ms. Second, the assumption of Keplerian (ballistic) trajectories requires that pressure forces in the bound ejecta remain small. However, r-process nucleosynthesis will, on timescales of order \sim second, heat the fallback, providing thermal pressure to frustrate fallback [80]. This is not entirely bad news for an extended emission model, though, since simulations of r-process heated fallback find, for sufficiently massive post-merger black holes ($> 6 - 8 M_{\odot}$, probably true for most BHNS post-mergers), a temporary pause in fallback rather than a permanent stop, which is closer to observed GRBs followed by extended emission than an uninterrupted power law [82]. From these two considerations, fallback and associated late-time emission may be complicated and Q -dependent.

Shocks at merger time allow the newborn disk to radiate neutrinos. The importance of weak interactions and neutrino emission depends on the mass accretion rate. If the accretion rate is above an ‘‘ignition threshold’’ of around $10^{-3} M_{\odot} \text{ s}^{-1}$, the disk will be efficiently neutrino cooled [130]. If not, it will be advective. Eventually, even a disk with initial \dot{M} will deplete sufficiently to fall below this level, and neutrino emission loses its thermal importance.

Weak interactions and the ignition threshold also determine the composition evolution. Initially, the disk matter is very neutron rich ($Y_e \approx 0.1$), like the neutron star it came from. Thus, $n + e^+$ reactions are more frequent than $p + e^-$ reactions (cf. Eq 1.5 and 1.6). The fraction of nucleons that are protons would then be expected to rise as electron antineutrino emission dominates over electron neutrino emission. This is, indeed, what simulations find in the early (~ 10 ms) post-merger evolution. After this, in efficiently neutrino cooled disks, Y_e begins to *decrease* again, settling back at around 0.1. The reason is that the equatorial density becomes high enough that the electron-positron gas becomes mildly degener-

ate: $\mu_{e^-}/k_B T \approx 1$. Equilibrium of electron-positron pair creation/annihilation forces $\mu_{e^+} = -\mu_{e^-}$. The electron and positron distribution functions differ only in the μ_{e^\pm}/kT term in the Fermi-Dirac function, so as the electron-positron gas starts to become degenerate, positrons become scarce compared to electrons, reducing the rate of $n + e^+ \rightarrow p + \bar{\nu}_e$ [131, 84]. The disk does not cool to become very degenerate ($\mu_{e^-}/k_B T \gg 1$) because strong degeneracy reduces the neutrino luminosity, causing the temperature to rise, so this process of approach to mild degeneracy with $Y_e \approx 0.1$ is self-regulating [131, 132, 130]. Below the ignition threshold, the degeneracy and regulation process does not operate. A bit later, as disk density and accretion rate decrease further, weak interactions effectively shut off to the extent that Y_e is frozen in fluid elements (as long as NSE persists). This extended post-neutrino phase will turn out to be crucial for outflows (see Section 1.9 below).

1.8 Magnetic field, jets, and gamma ray bursts

MHD simulations of BHNS post-merger evolution focus both on the magnetic field’s role in causing the turbulent “viscosity” and in the generation of polar jets. If the jet is generated by the Blandford-Znajek mechanism, the power output L_{BZ} will be proportional to Φ^2 , where Φ is the magnetic flux on the black hole horizon:

$$\Phi = \int_H |B \cdot n| dA \quad (1.10)$$

(Without the absolute value sign, field lines going in the horizon in one hemisphere would cancel field lines coming out the other.) Thus, powerful jets require large magnetic flux on the horizon. Accretion from the disk can advect onto the horizon, and this flux can accumulate with time. The pressure of the surrounding disk is also needed to confine the near-horizon field. If the flux reaches $\Phi = \Phi_{\text{MAD}} \approx 50 \dot{M}^{1/2} M_{\text{BH}}$, the field will be strong enough to oppose further accretion, leading to a magnetically arrested disk (MAD) state [133, 134]. MAD accretion releases energy very efficiently, but since once Φ reaches Φ_{MAD} it is subsequently stuck at $\Phi \approx \Phi_{\text{MAD}}$, the subsequent L_{BZ} is tied to the (declining) mass accretion rate.

During and shortly after merger, several processes will amplify the magnetic field inside the incipient disk. First, the field will grow due to *magnetic winding* (also called the “ ω -effect” in dynamo literature): as a simple consequence of the fact that magnetic field lines are “frozen into” a conducting fluid, differential rotation/shear will “wind up” field lines. Winding will lead to a linear in time growth of the toroidal component of the field (B^ϕ).

The other sources of magnetic field growth are MHD instabilities. For example, as tidal disruption turns the star into a stream swirling around the black hole, this wound spiral arm shears against itself, triggering the Kelvin-Helmholtz instability (KHI). Vortices will form the shear interface in which magnetic fields will quickly wind up [95, 135].

The most well-known is the *MRI*, which is triggered in a rotating, conducting, weakly magnetized ($B^2 \ll P$) fluid whenever

$$\varpi \partial_{\varpi} \Omega^2 + N^2 < 0, \quad (1.11)$$

where ϖ is the cylindrical radius (distance from the orbital axis), Ω is the orbital angular frequency, and N is the Brunt-Väisälä frequency [136]. In a disk, the first term will dominate, and since Ω^2 always decreases with ϖ in disks, the condition will be satisfied. The MRI is a linear instability leading to exponential growth at rate $\sim \Omega$ of the B-field. The fastest growing unstable mode has wavelength $\lambda_{\text{MRI}} \sim v_A/\Omega$, where $v_A = B/\sqrt{4\pi\rho}$ is the Alfvén speed. Thus, stronger fields (so long as they are not strong enough to suppress the MRI) have larger λ_{MRI} , and numerical relativity simulations usually insert unphysically large initial magnetic fields of order 10^{16} G in order to be able to numerically resolve the MRI in the subsequent merger. This is justified by pointing out that the inserted magnetar-level field is still dynamically weak in the disk ($B^2/P \sim 10^{-2}$), in that there is much room for it to grow to reach equipartition, so hopefully details of the seed field will not imprint the field when it has saturated.

The MRI drives turbulence, whereby energy injected at λ_{MRI} cascades to smaller scales, and if one does not resolve a sufficient portion of the inertial range at scales beneath λ_{MRI} , turbulent transport effects might be improperly modeled. The highest resolution MHD BHNS simulations, by Kiuchi *et al* [95] and by Izquierdo *et al* [135] (minimum grid spacing 0.12 km, the latter study including subgrid turbulence modeling, both studies omitting neutrinos) fail to demonstrate numerical convergence, with the former studying finding at higher resolution much greater near-BH disk heating and early-time outflow rate and the latter study much faster initial magnetic field growth driven by the KHI.

Early BHNS merger simulations with MHD took the initial magnetic field to consist of poloidal loops with axis aligned with the orbit and with field confined inside the neutron star. These simulations found that the field in the post-merger disk quickly wound into a toroidally dominated configuration, with no observable jets, at least on the tens of millisecond timescales investigated [75, 137, 138]. (However, MRI-generated poloidal field can dominate in parts of the low density region [139].) Simulations of black hole accretion disks have looked into the differences when one begins with a poloidal vs. a toroidal seed field. While the MRI inside the disk is found to be similar in both cases, jet launching requires poloidal magnetic field reaching the black hole [140]. Thus, it is not surprising that these toroidal field-dominated merger outcomes did not quickly produce jets.

The University of Illinois Urbana-Champaign group has investigated the effect of the geometry of the neutron star's initial magnetic field on the post-merger field. If the confined magnetic field is tilted with respect to the orbital axis, there can be a somewhat larger early post-merger poloidal fields, but still insufficient to generate an early post-merger jet [138]. On the other hand, jets can more quickly (≈ 100 ms) emerge from a BHNS merger involving a neutron star with pre-merger poloidal field extending outside the neutron star, because in such a case more magnetic field

survives the merger and can be wound above the poles into an incipient jet [141, 142]. These were, in fact, the first BHNS simulations to successfully demonstrate jet formation.

Jets are still possible for disks with toroidal initial fields, but there is the delay that the disk must first generate a poloidal field by *dynamo* action, the process whereby some of the toroidal field can be converted through small-scale turbulence into a large-scale poloidal field [144]. Magnetic winding feeds poloidal field into toroidal field, so the dynamo can be a self-sustaining cycle. Distinctive oscillatory behavior is seen in the large-scale dynamo-driven field. In black hole accretion systems, one can see a cyclic drift in the latitude of toroidal field strength reminiscent of the “butterfly diagrams” in solar sunspots [145, 31]. Disk simulations with toroidal initial field find that dynamo poloidal field growth can indeed happen [146, 147], although the jets that eventually form might be more intermittent (“striped”) than those from disks with poloidal seed field [147].

A few very recent simulations have followed magnetized BHNS disks for second timescales: the work of Hayashi *et al* [31, 148] using the SACRA code and the work of Gottlieb *et al* [143, 149] using the H-AMR code with initial data from hydrodynamic BHNS mergers with the SPec code. The two studies differed in several ways. Notably, the SACRA simulations included neutrino effects and recombination while the H-AMR simulations did not, but the H-AMR simulations evolved for longer times. Here, we will present the main points of the picture emerging from extended post-merger MHD simulations, encouraging readers to consult the original papers for details. Readers should note that some papers only insert a seed magnetic field after merger (e.g. [150, 143, 149]). Magnetized BHNS mergers find that the field in the initial post-merger disk is predominantly toroidal, so the early evolution of disks with poloidal seed field should not be trusted much. Also, electromagnetic luminosity can be reported differently, e.g. Poynting luminosity across the whole horizon, a measure of electromagnetic energy extraction from the black hole, vs. isotropic equivalent luminosity to the Poynting flux near the axis, a measure of jet strength relevant to an on-axis observer.

Dynamo activity is clearly seen in extended MHD simulations of BHNS disks, both in the growth of poloidal field and in the distinctive “butterfly” effect drift in the toroidal field [31, 148]). The polar region after merger is not empty but contains matter ejected during tidal disruption and merger as well as early-time disk outflows. This delays the formation of a magnetosphere until the density inside a funnel region falls to $\rho < b^2/8\pi$ [139, 31], and the incipient jet must push through a cocoon of this matter [143].

The horizon magnetic flux Φ , and hence the Poynting luminosity for the Blandford-Znajek effect, accumulates early and is fairly constant for order seconds, excepting fluctuations due to turbulence and dynamo cycles. During this time, the disk depletes, and the accretion rate falls off like $\dot{M} \propto t^{-2}$. Thus the MAD criterion ratio $\Phi/(M\dot{M}_{\text{BH}})$ grows. Eventually, it is inevitable that the disk will enter a MAD state. The nominal efficiency of accretion (L_{BZ}/\dot{M}) grows (“output” holding steady while “input” decreases), reaching order unity as the disk reaches MAD state. As \dot{M} drops, gas pressure at the edge of the funnel region decreases, so the gas loses ability to

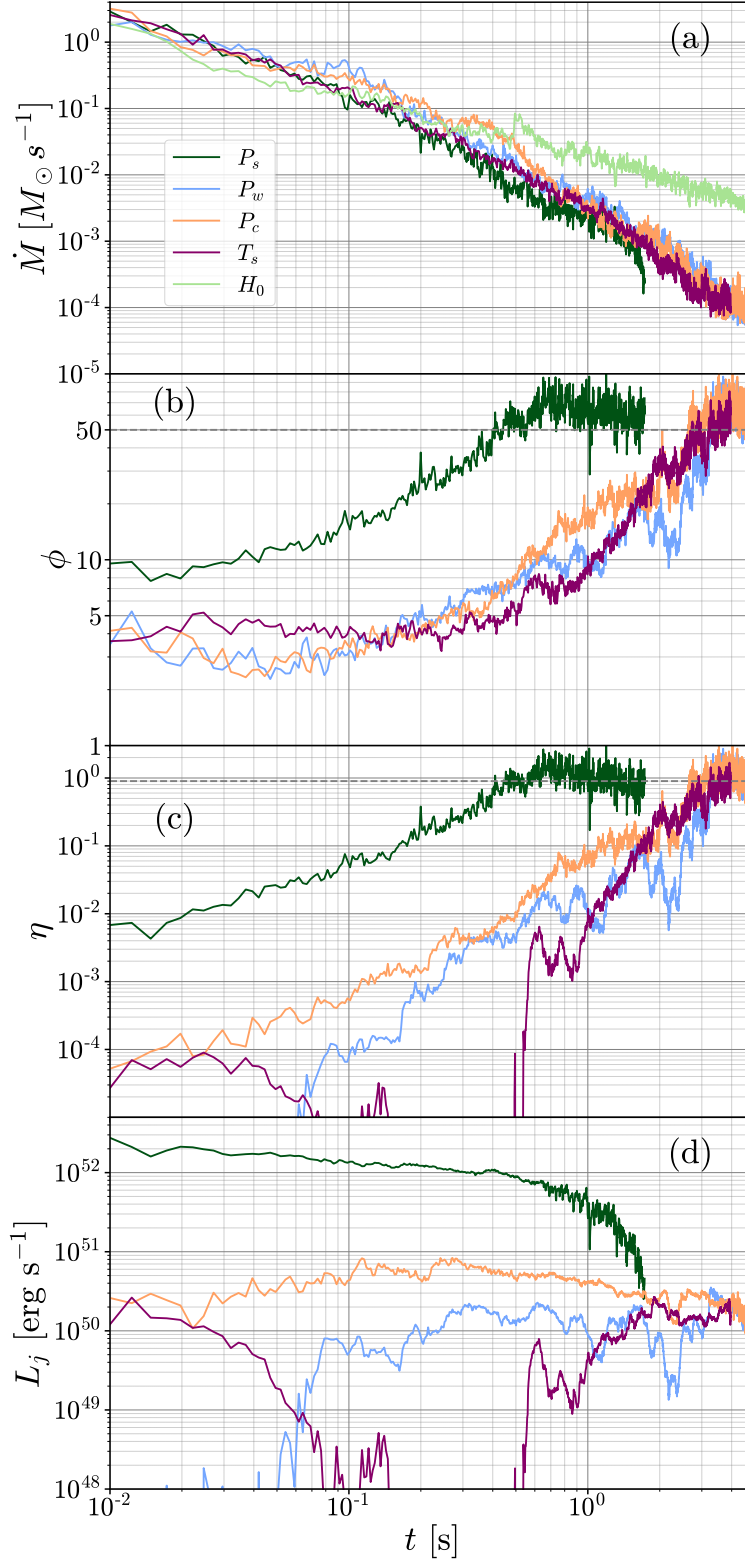


Fig. 1.5: Electromagnetic energy extraction (measured at $r = 5M_{\text{BH}}$) for a $Q = 2$, $\chi_{\text{BH}} = 0.6$ system with different choices of magnetic field inserted post-merger. Figure from Gottlieb *et al* [143] under the terms of the Creative Commons Attribution 4.0 International License. **Panel (a)**: Mass accretion rate **Panel (b)**: Dimensionless magnetic flux $\phi = \Phi / \sqrt{MM_{\text{BH}}^2}$, where Φ is the magnetic flux. Ultimately, all models turn MAD when $\phi \approx 50$ (dashed line). **Panel (c)**: The jet launching efficiency **Panel (d)**: The jet luminosity, $L_j = \eta \dot{M}$

confine the jet. Even before the MAD criterion is satisfied, this loss of confining pressure causes the jet to broaden, leading to a corresponding decrease of flux observed by an observer in the jet’s path [31]. Once the disk becomes MAD, the jet luminosity is constrained to decrease along with \dot{M} at a rate $\propto t^{-2}$, which we should be able to observe in short GRBs. These features of the evolution are shown in Figure 1.5.

If it is true that the ultimate falloff of GRB jet luminosity is caused by the growing relative strength of magnetic forces on a depleting disk, then there is a connection between the post-merger disk mass (which determines \dot{M}), the jet luminosity, and the lifetime after which the jet luminosity drops, as illustrated in Figure 1.5. For a given disk mass (and hence $\dot{M}(t)$), a more luminous jet would reach this time at which decay commences sooner. Considering only the MAD criterion, this is when the L_{BZ} and \dot{M} curves cross [149].

Magnetic fields are not the only mechanism that has been considered for launching jets. Another energy source comes from the annihilation of neutrinos and antineutrinos in the (neutrino) optically-thin polar region. The luminosity from neutrino annihilation for a hot, high \dot{M} (but neutrino transparent) disk is roughly $L_{\nu\bar{\nu}} \sim 10^{52} (\dot{M}/M_{\odot} s^{-1})^{2.25} \text{ erg s}^{-1}$ [151]. For high accretion rates, of order a percent of the neutrino luminosity can be deposited in this way, but naturally, this source of energy shuts off when the accretion rate drops below the weak interaction ignition accretion rate, and is probably negligible for $\dot{M} < 10^{-2} M_{\odot} s^{-1}$ [152]. This is one problem for the $\nu\bar{\nu}$ GRB model. Another obstacle to relativistic jets is the inertia of matter ejected during merger polluting the polar regions (“baryon loading”). Radiative hydrodynamic evolutions suggest that this ejecta will prevent $\nu\bar{\nu}$ annihilation from accelerating polar outflows to relativistic speeds in NSNS remnants [153]. The same paper concludes that BHNS disks (which have somewhat cleaner polar regions after merger) can produce GRB fireballs, but the energies and durations are too low to explain most short GRBs. It remains possible that the neutrino mechanism is important early on. Since, according to high resolution MHD BHNS simulations, magnetic jets take at least tens of milliseconds to form [95], the character of the relativistic outflow might change from fireball to Poynting flux dominated (cf. [154]). It should also be remembered that, even if $\nu\bar{\nu}$ annihilation cannot drive a relativistic outflow, it might contribute to mildly relativistic winds (cf. [155]), a topic to which we now turn.

1.9 Outflows, Kilonovae, and Radio Flares

Matter from the neutron star that ends up being ejected will decompress and evolve into some kind of “normal” matter; this evolution turns out to be of great interest for electromagnetic signals and production of heavy elements. When ρ and T are low enough that outgoing gas leaves NSE, many nucleons will have collected into heavy nuclei. However, if Y_e is low (many more neutrons than protons), there will be a large number of “extra” free neutrons as well. In this case, nuclei will rapidly

capture neutrons, bringing them close to the neutron drip line, i.e. the most neutrons a nucleus can hold for given number of protons—on a space of isotopes labeled by (A, Z) , the maximum of A for given Z . These nuclei can eventually form the “r-process” elements. The distribution of nuclei produced by the r-process has three peaks at $A \sim 70\text{--}80$, $120\text{--}130$, and $190\text{--}200$. Notably, it produces lanthanides and actinides (located past the second peak). Absent rapid neutron capture (i.e. for higher Y_e), nuclei stay closer to the valley of stable isotopes (a swath in the $A\text{--}Z$ plane); there can be s-process nucleosynthesis in this regime. For high- Y_e outflow, the r-process does not proceed far enough to produce significant amounts of elements beyond the second or even first peak; in particular lanthanides and actinides are not efficiently produced.

The possibility that tidal disruption in BHNS mergers could produce a large mass of unbound outflow which might then undergo r-process nucleosynthesis was pointed out by Lattimer and Schramm in 1976 [156]. Li and Paczynski noticed that radioactive decays in ejecta could power a bright electromagnetic transient [157]. However, it was only sometime afterward that models were created with realistic heating rates and opacities [80, 158, 159, 160]. Opacity turns out to be crucial—a more opaque gas will trap photons longer, so that they escape on a longer timescale and at lower energy. Lanthanides, if present, introduce a thicket of absorption lines due to their partially-filled valence f shells, greatly increasing the bound-bound opacity. A lanthanide-rich ejecta glows in the near infrared on timescale of a week (“red kilonova”); a lanthanide-poor ejecta glows in the optical-UV on day timescale (“blue kilonova”). The transition between one and the other is at about $Y_e \approx 0.25$ [161, 162, 163].

As the outflow spreads and decompresses further, it interacts with the background interstellar medium (ISM); electrons are accelerated in the shock moving into the ISM and emit synchrotron radiation. This results in a distinct signal, a radio flare lasting years to decades [164, 165, 166]. This long timescale is set by the deceleration time, the time it takes the ejecta to sweep up roughly its own mass in ISM. The timescale and strength of these flares depends both on the kinetic energy of the ejecta and the density of the surrounding ISM. Thus, the properties of outflows determine multiple signals.

Numerical simulations predict the mass of outflow and its distribution in speed, entropy, and Y_e . One issue is how to identify unbound matter. In a stationary spacetime, u_t is constant on geodesics, so a $u_t < -1$ geodesic can be identified as unbound. Furthermore, $-u_t$ can be identified as the asymptotic Lorentz factor. However, the spacetime is not stationary in the early merger, and—a more serious problem—the outflow is not geodesic, at least within the grid and timeframe which most simulations can afford to maintain, because of the persistence of pressure forces (e.g. [167]). In a stationary flow (not necessarily geodesic), the Bernoulli parameter hu_t is constant on fluid elements. At asymptotically large distances and late times, $\rho_0 \rightarrow 0$, $h \rightarrow h_\infty$, so for such a flow, one can tag $(h/h_\infty)u_t < -1$ fluid elements as unbound and $-(h/h_\infty)u_t$ as the asymptotic Lorentz factor, but, unfortunately, the outflow is not stationary either. One must also worry about the effect of r-process heating, currently not accounted for in most merger and post-merger simulations.

For more on the subtleties of identifying unbound matter and its asymptotic speed, see Foucart *et al* [168].

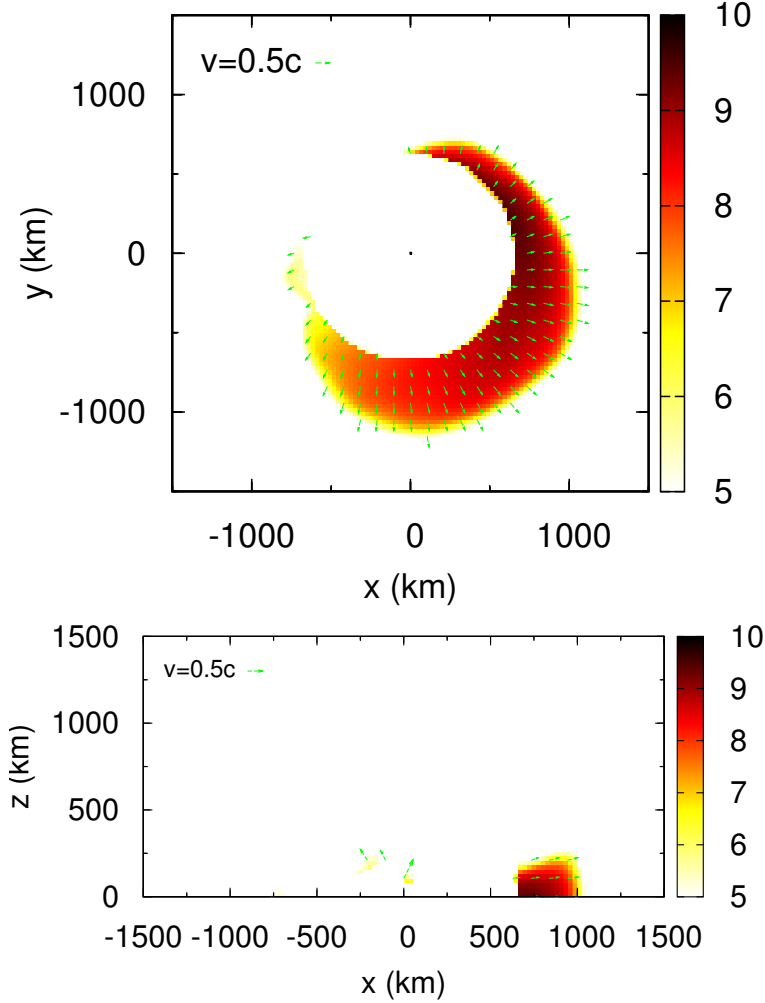


Fig. 1.6: Concentration of dynamical ejecta for a $Q = 5$, $\chi_{\text{BH}} = 0.75$, aligned spin BHNS merger. **Top:** equatorial plane. **Bottom:** a meridional plane. Color indicates density. Reprinted figure with permission from Kyutoku, Ioka, and Shibata, Phys. Rev. D **88**, 041503 (2013) [169]. Copyright 2013 by the American Physical Society.

Newtonian and relativistic simulation confirm that BHNS mergers produce large ejecta masses, up to $\sim 10^{-1}M_{\odot}$ [170, 169, 28, 121, 119, 89, 85]. Dynamical ejecta masses can thus be much larger than in NSNS systems, mainly because of the higher

mass ratios Q for BHNS binaries, rather than because of something distinctive about the presence of a black hole. (Asymmetric NSNS systems also tend to produce more dynamical ejecta than equal mass systems.) Since the ejecta is produced by tidal disruption of the neutron star before merger, the ejecta is cold and little affected by neutrino (weak interaction) processes [89, 171], so its electron fraction is essentially what it was in the pre-merger neutron star, about $Y_e \approx 0.05$. Such extremely neutron-rich material will produce 2nd and 3rd peak r-process elements and produce a red kilonova. Typical asymptotic velocities are $\sim 0.2\text{--}0.3c$. BHNS dynamical ejecta is extremely anisotropic, much more so than NSNS ejecta, with outflow concentrated within 20° of the equatorial plane and sweeping out only about half of this plane (180°). (See Fig. 1.6.) The ejecta thus has an overall linear momentum, so the black hole remnant can get a kick of $\sim 100\text{ km s}^{-1}$, a larger effect than the gravitational wave recoil [169, 28, 121]. Further consequences of this overall direction of ejecta motion will be discussed below. It should be pointed out, though, that BHNS systems with significantly misaligned black hole spin can produce dynamical ejecta extending over 360° [123].

An additional component of outflow comes later from the accretion disk, especially after neutrino cooling has diminished in importance, and the disk has become advective. These disk wind outflows have been studied in Newtonian physics in 2D, with the black hole modeled as a central potential and MHD turbulence modeled as a shear viscosity, in a series of papers by Fernandez and collaborators [172, 173, 129, 174, 175]. There have also been a small number of 2D relativistic viscous hydrodynamic studies, which find qualitatively similar results [176, 177, 167]. Outflow gas is unbound from the disk by thermal pressure, so the key to understanding disk winds is to understand how thermal energy is added to the disk. Viscosity provides the major source of heating; since viscosity is considered a model for turbulence, this viscous heating can be interpreted as dissipation of turbulent energy on small scales. Heat generated in the interior of the disk can trigger convection which transports this heat to the surface. (Thus, even simulations which don't explicitly include magnetorotational turbulence often show disk snapshots which look quite turbulent.) Thermal energy is also boosted by recombination of nucleons into nuclei, with the accompanying release of nuclear binding energy. (Recall, this is not technically "heating" since it is reversible and adiabatic so long as the fluid remains in NSE. It is automatically included in simulations that use temperature-dependent equations of state and use a conservative formulation of the fluid or MHD equations.)

A significant fraction of the disk's mass can be ejected in these winds, with 10% to 20% of the initial disk mass being typical. An exploration of the parameter space of disks [175] shows that the fraction of disk mass ejected decreases with the compactness of the initial disk (proportional to the black hole mass divided by the radius of the initial density peak). The dependence on disk compactness can be understood by remembering that most of the outflow launching happens after weak interaction freeze-out, when accretion becomes advective. For a more compact disk, more of the mass will accrete before this time, meaning that for a less compact disk, more mass will be remaining when strong outflows commence. Ejected mass fraction also

decreases with the initial disk mass. Ejecta from disk outflows is found to be significantly slower than dynamical ejecta, with $v \approx 0.05c$ being a typical measurement. Unlike the dynamical ejecta, this ejecta undergoes significant neutrino processing from its time in the disk, and average $Y_e \approx 0.3$. Of course, within the disk outflow from a single merger, there will be gas with a range of Y_e , but more than half will be lanthanide and actinide-poor and thus lower opacity.

Viscous hydrodynamics is an approximation meant to model MHD turbulence. How well outflows from viscous evolution match those of full MHD evolution has been tested by comparing results of 3D MHD simulations to those of 2D viscous hydrodynamics, with both simulation types including neutrino cooling and nuclear recombination. One finds that MHD simulations produce late-time thermal winds that are very similar in mass, velocity, and composition to the outflows in 2D viscous hydrodynamics simulations for alpha viscosity in the range $\alpha_{\text{SS}} \approx 0.03\text{--}0.1$. Simulations with poloidal initial field (with ratio of gas pressure to magnetic pressure of $\beta \sim 10^2$) find an additional, early-time magnetically-driven ejecta, amounting to another 20% of the disk's mass, with higher velocity and lower Y_e than the later wind [30]. This early-time outflow is, however, sensitive to the choice of seed field [147]. It is essentially removed if the initial poloidal field is weak ($\beta \sim 10^3$) or if the initial field is toroidal. BHNS merger MHD simulations indicate the early post-merger field is in fact predominantly toroidal, and one does not observe the early outflow in these simulations [31]. (However, outflow might appear only at sufficiently high resolution [95], so one should be cautious with these conclusions.)

We have seen that disrupting BHNS mergers will, except for systems with low-mass black holes, have as much or more dynamical ejecta than disk ejecta. Furthermore, we have seen that the dynamical ejecta can be highly asymmetric—often concentrated near the orbital equator and to one side. Both the mass and asymmetry of dynamical ejecta distinguish typical BHNS from typical NSNS outflows. They have observable consequences.

Consider the asymmetry of ejecta. The flatness of the ejecta means photons are able to random walk to the vertical surface faster than they would be able to escape a spherical distribution. This results in a shorter time to peak emission, higher ejecta temperature at this time, higher peak luminosity, and bluer emission [169, 178]. It has even been suggested that the difference in color for a given luminosity might provide a way to distinguish BHNS from NSNS mergers from their kilonovae [178]. The asymmetry of ejecta motion, on the other hand, causes Doppler effects, so that the brightness and color depends on the viewing angle—whether the ejecta is moving toward or away from the observer [179].

The overall kilonova emission will depend on emission from and opacity of both dynamical and disk outflow components and their spatial arrangement. The dynamical ejecta will be farther out from the black hole and equatorially concentrated, while the disk outflow will be more isotropic. Thus, there may be a low-opacity disk outflow producing a blue emission, but it might only be visible from certain viewing angles, because in equatorial directions, the blue emission is blocked by the more-opaque dynamical ejecta between the disk outflow and the viewer. Some

work has been done in figuring out how the different ejecta component effects combine at different viewing angles to produce overall light curves [129, 174, 180, 181].

The distinct features of BHNS dynamical ejecta also affect the later radio flare. A flat outflow takes longer than a spherical outflow of the same mass to sweep up its own mass, so the peak time might be delayed. Also, the overall motion of the ejecta in one direction results in a proper motion of the radio source which could possibly be detected [169].

1.10 Conclusions

BHNS mergers involve physics similar to that of NSNS mergers and have the potential to produce similar types of signals. They are distinguished from NSNS mergers in that higher mass ratio Q is expected, the post-merger central remnant is definitely a black hole, the black hole is likely more massive than that produced by NSNS post-merger collapse, greater dynamical ejecta masses are possible, this dynamical ejecta is colder, more neutron-rich, and more anisotropic, and the post-merger polar region is likely to be less baryon loaded. These differences may have observational consequences. The challenge of MHD simulations comes from the range of time and length scales that must be covered. However, general aspects of the merger and post-merger evolution are coming to be known with confidence, because they follow from general principles: the dependence of tidal disruption on binary parameters, the early importance but eventual shut-off of neutrino-emitting weak interactions, and the natural evolution of the disk toward a magnetically arrested state.

Nevertheless, no current simulation of the post-merger evolution should be considered definitive, because none contains all of the ingredients needed to be fully trustworthy. MHD and neutrino emission are both crucial to the post-merger emission, and while many studies include one or the other, few include them both. Those of which the author is aware include [150, 139, 31, 148]. The first two of these used neutrino leakage, which is only quantitatively reliable for optically thin disks. However, even including both magnetic fields and neutrino transport is insufficient. First, there are the difficulties of resolving turbulence induced by the MRI. Convergence studies without neutrino effects (which are thus *physically* unreliable) indicate that grid spacing of $\Delta x < 0.2$ km is needed to capture early outflows [95]. The studies cited above that include neutrino effects do not see these outflows or this resolution sensitivity, but they also have not gone to such high resolution. Furthermore, the neutrino treatment in these studies did not include neutrino-antineutrino annihilation and flavor oscillations. Simulations continuing for seconds and tracking ejecta to large distances face the more important problem of the breakdown of nuclear statistical equilibrium, which (because of r-process heating) cannot adequately be relegated to post-processing.

In addition to these modeling issues, future simulations must more adequately explore the BHNS parameter space. Much of the work reviewed in this chapter has concentrated on low-to-moderate mass ratio systems with “canonical” neutron star

masses of $1.3\text{--}1.4M_{\odot}$ and aligned black hole spin. Properly calibrating BHNS gravitational wave models will require more adequately sampling a fuller range of the possible masses and spins. We should be sure, for example, that the conclusions we have drawn regarding characteristically asymmetric BHNS ejecta are not too sensitive to an assumption that the black hole spin misalignment angle is small. We should be careful in extrapolating the conclusions of our few seconds-long MHD simulations [148, 143] carried out from two sets of masses and spins to the whole range of disrupting BHNS systems. As daunting as the task may be, we must carry out seconds-long radiation MHD simulations covering a wide range of BHNS systems.

Acknowledgements I am grateful to Francois Foucart, Ore Gottlieb, Koutarou Kyutoku, Nishad Muhammed, Stuart Shapiro, and Samuel Tootle for viewing a draft and providing useful comments. I also thank the authors of references [51], [109], and [169] for permission to reuse figures 1.3, 1.4, and 1.6. I am grateful for support from the NSF through grant PHY-2110287 and from NASA through grant 80NSSC22K0719.

References

1. R. Abbott, et al., Observation of Gravitational Waves from Two Neutron Star–Black Hole Coalescences. *Astrophys. J. Lett.* **915**(1), L5 (2021). <https://doi.org/10.3847/2041-8213/ac082e>. [arXiv:2106.15163](https://arxiv.org/abs/2106.15163) [astro-ph.HE]
2. R. Abbott, et al., GWTC-3: Compact Binary Coalescences Observed by LIGO and Virgo during the Second Part of the Third Observing Run. *Phys. Rev. X* **13**(4), 041,039 (2023). <https://doi.org/10.1103/PhysRevX.13.041039>. [arXiv:2111.03606](https://arxiv.org/abs/2111.03606) [gr-qc]
3. R. Abbott, et al., GWTC-2.1: Deep extended catalog of compact binary coalescences observed by LIGO and Virgo during the first half of the third observing run. *Phys. Rev. D* **109**(2), 022,001 (2024). <https://doi.org/10.1103/PhysRevD.109.022001>. [arXiv:2108.01045](https://arxiv.org/abs/2108.01045) [gr-qc]
4. J.P. Zhu, S. Wu, Y. Qin, B. Zhang, H. Gao, Z. Cao, Population Properties of Gravitational-wave Neutron Star–Black Hole Mergers. *Astrophys. J.* **928**(2), 167 (2022). <https://doi.org/10.3847/1538-4357/ac540c>. [arXiv:2112.02605](https://arxiv.org/abs/2112.02605) [astro-ph.HE]
5. M. Linares, T. Shahbaz, J. Casares, Peering into the dark side: Magnesium lines establish a massive neutron star in PSR J2215+5135. *Astrophys. J.* **859**(1), 54 (2018). <https://doi.org/10.3847/1538-4357/aabde6>. [arXiv:1805.08799](https://arxiv.org/abs/1805.08799) [astro-ph.HE]
6. H.T. Cromartie, et al., Relativistic Shapiro delay measurements of an extremely massive millisecond pulsar. *Nature Astron.* **4**(1), 72–76 (2019). <https://doi.org/10.1038/s41550-019-0880-2>. [arXiv:1904.06759](https://arxiv.org/abs/1904.06759) [astro-ph.HE]
7. C.E. Rhoades, R. Ruffini, Maximum Mass of a Neutron Star. *Phys. Rev. Lett.* **32**(6), 324–327 (1974). <https://doi.org/10.1103/PhysRevLett.32.324>
8. F.J. Fattoyev, C.J. Horowitz, J. Piekarewicz, B. Reed, Gw190814: Impact of a 2.6 solar mass neutron star on the nucleonic equations of state. *Phys. Rev. C* **102**, 065,805 (2020). <https://doi.org/10.1103/PhysRevC.102.065805>. URL <https://link.aps.org/doi/10.1103/PhysRevC.102.065805>
9. R. Essick, P. Landry, Discriminating between Neutron Stars and Black Holes with Imperfect Knowledge of the Maximum Neutron Star Mass. *Astrophys. J.* **904**(1), 80 (2020). <https://doi.org/10.3847/1538-4357/abbd3b>. [arXiv:2007.01372](https://arxiv.org/abs/2007.01372) [astro-ph.HE]

10. R. Abbott, et al., Population of Merging Compact Binaries Inferred Using Gravitational Waves through GWTC-3. *Phys. Rev. X* **13**(1), 011,048 (2023). <https://doi.org/10.1103/PhysRevX.13.011048>. [arXiv:2111.03634](https://arxiv.org/abs/2111.03634) [astro-ph.HE]
11. B.D. Metzger, Kilonovae. *Living Rev. Rel.* **23**(1), 1 (2020). <https://doi.org/10.1007/s41114-019-0024-0>. [arXiv:1910.01617](https://arxiv.org/abs/1910.01617) [astro-ph.HE]
12. E. Nakar, Short-hard gamma-ray bursts. *Phys. Rep.* **442**, 166–236 (2007). <https://doi.org/10.1016/j.physrep.2007.02.005>. [arXiv:astro-ph/0701748](https://arxiv.org/abs/astro-ph/0701748)
13. E. Troja, et al., A nearby long gamma-ray burst from a merger of compact objects. *Nature* **612**(7939), 228–231 (2022). <https://doi.org/10.1038/s41586-022-05327-3>. [arXiv:2209.03363](https://arxiv.org/abs/2209.03363) [astro-ph.HE]
14. A.J. Levan, et al., Heavy-element production in a compact object merger observed by JWST. *Nature* **626**(8000), 737–741 (2024). <https://doi.org/10.1038/s41586-023-06759-1>. [arXiv:2307.02098](https://arxiv.org/abs/2307.02098) [astro-ph.HE]
15. J.P. Norris, J.T. Bonnell, Short gamma-ray bursts with extended emission. *Astrophys. J.* **643**, 266–275 (2006). <https://doi.org/10.1086/502796>. [arXiv:astro-ph/0601190](https://arxiv.org/abs/astro-ph/0601190)
16. E. Berger, Short-Duration Gamma-Ray Bursts. *Ann. Rev. Astron. Astrophys.* **52**, 43–105 (2014). <https://doi.org/10.1146/annurev-astro-081913-035926>. [arXiv:1311.2603](https://arxiv.org/abs/1311.2603) [astro-ph.HE]
17. S. Nissanke, M. Kasliwal, A. Georgieva, Identifying Elusive Electromagnetic Counterparts to Gravitational Wave Mergers: an end-to-end simulation. *Astrophys. J.* **767**, 124 (2013). <https://doi.org/10.1088/0004-637X/767/2/124>. [arXiv:1210.6362](https://arxiv.org/abs/1210.6362) [astro-ph.HE]
18. M. Bhattacharya, P. Kumar, G. Smoot, Mergers of black hole–neutron star binaries and rates of associated electromagnetic counterparts. *Mon. Not. Roy. Astron. Soc.* **486**(4), 5289–5309 (2019). <https://doi.org/10.1093/mnras/stz1147>. [arXiv:1809.00006](https://arxiv.org/abs/1809.00006) [astro-ph.HE]
19. L.S. Collaboration, V. Collaboration, F. GBM, INTEGRAL, I. Collaboration, A.C.Z.T.I. Team, I. Collaboration, I.H. Collaboration, A. Collaboration, S. Collaboration, A. Team, M. Team, D.E.C.G.E. Collaboration, D. Collaboration, D. Collaboration, G.W.I. TeAm, F.L.A.T. Collaboration, A.T.C. Array, A.S. Pathfinder, L.C.O. Group, OzGrav, DWF, AST3, C. Collaborations, V. Collaboration, M. Collaboration, J-GEM, GROWTH, JAGWAR, Caltech-NRAO, TTU-NRAO, N. Collaborations, Pan-STARRS, M. Team, T. Consortium, K. Collaboration, N.O. Telescope, ePESSTO, GROND, T.T. University, S. Group, T.R.O. of the South Collaboration, B. Collaboration, MWA, M.W. Array, C. Collaboration, I.G.F. up Collaboration, H.E.S.S. Collaboration, L. Collaboration, L.W. Array, H. Collaboration, P.A. Collaboration, A. Collaboration, E.V. Team, P. of the Sky Collaboration, C.T. at McGill University, D.F. Network, ATLAS, H.T.R.U. Survey, RIMAS, RATIR, S.S. Africa/MeerKAT, Multi-messenger Observations of a Binary Neutron Star Merger. *Astrophys. J.* **848**, L12 (2017). <https://doi.org/10.3847/2041-8213/aa91c9>. [arXiv:1710.05833](https://arxiv.org/abs/1710.05833) [astro-ph.HE]
20. O. Gottlieb, E. Nakar, T. Piran, The cocoon emission – an electromagnetic counterpart to gravitational waves from neutron star mergers. *Mon. Not. Roy. Astron. Soc.* **473**(1), 576–584 (2018). <https://doi.org/10.1093/mnras/stx2357>. [arXiv:1705.10797](https://arxiv.org/abs/1705.10797) [astro-ph.HE]
21. D. Lazzati, R. Perna, Jet-Cocoon Outflows from Neutron Star Mergers: Structure, Light Curves, and Fundamental Physics. *Astrophys. J.* **881**(2), 89 (2019). <https://doi.org/10.3847/1538-4357/ab2e06>. [arXiv:1904.08425](https://arxiv.org/abs/1904.08425) [astro-ph.HE]
22. O. Gottlieb, D. Issa, J. Jacquemin-Ide, M. Liska, A. Tchekhovskoy, F. Foucart, D. Kasen, R. Perna, E. Quataert, B.D. Metzger, Hours-long Near-UV/Optical Emission from Mildly Relativistic Outflows in Black Hole–Neutron Star Mergers. *Astrophys. J. Lett.* **953**(1), L11 (2023). <https://doi.org/10.3847/2041-8213/acec4a>. [arXiv:2306.14946](https://arxiv.org/abs/2306.14946) [astro-ph.HE]
23. K. Kyutoku, M. Shibata, K. Taniguchi, Coalescence of black hole–neutron star binaries. *Living Rev. Rel.* **24**(1), 5 (2021). <https://doi.org/10.1007/s41114-021-00033-4>. [arXiv:2110.06218](https://arxiv.org/abs/2110.06218) [astro-ph.HE]

24. F. Foucart, *Black Hole-Neutron Star Mergers* (Springer Nature Singapore, Singapore, 2022), pp. 611–660. https://doi.org/10.1007/978-981-16-4306-4_14. URL https://doi.org/10.1007/978-981-16-4306-4_14
25. D. Tsang, Shattering Flares During Close Encounters of Neutron Stars. *Astrophys. J.* **777**, 103 (2013). <https://doi.org/10.1088/0004-637X/777/2/103>. arXiv:1307.3554 [astro-ph.HE]
26. M. Vallisneri, Prospects for gravitational wave observations of neutron star tidal disruption in neutron star / black hole binaries. *Phys. Rev. Lett.* **84**, 3519 (2000). <https://doi.org/10.1103/PhysRevLett.84.3519>. arXiv:gr-qc/9912026
27. F. Foucart, M.B. Deaton, M.D. Duez, E. O’Connor, C.D. Ott, R. Haas, L.E. Kidder, H.P. Pfeiffer, M.A. Scheel, B. Szilagyi, Neutron star-black hole mergers with a nuclear equation of state and neutrino cooling: Dependence in the binary parameters. *Phys. Rev. D* **90**, 024,026 (2014). <https://doi.org/10.1103/PhysRevD.90.024026>. arXiv:1405.1121 [astro-ph.HE]
28. F. Foucart, M.B. Deaton, M.D. Duez, L.E. Kidder, I. MacDonald, C.D. Ott, H.P. Pfeiffer, M.A. Scheel, B. Szilagyi, S.A. Teukolsky, Black hole-neutron star mergers at realistic mass ratios: Equation of state and spin orientation effects. *Phys. Rev.* **D87**, 084,006 (2013). <https://doi.org/10.1103/PhysRevD.87.084006>. arXiv:1212.4810 [gr-qc]
29. N.I. Shakura, R.A. Sunyaev, in *X- and Gamma-Ray Astronomy, IAU Symposium*, vol. 55, ed. by H. Bradt, R. Giacconi (1973), p. 155
30. R. Fernández, A. Tchekhovskoy, E. Quataert, F. Foucart, D. Kasen, Long-term GRMHD simulations of neutron star merger accretion discs: implications for electromagnetic counterparts. *Mon. Not. Roy. Astron. Soc.* **482**(3), 3373–3393 (2019). <https://doi.org/10.1093/mnras/sty2932>. arXiv:1808.00461 [astro-ph.HE]
31. K. Hayashi, S. Fujibayashi, K. Kiuchi, K. Kyutoku, Y. Sekiguchi, M. Shibata, General-relativistic neutrino-radiation magnetohydrodynamic simulation of seconds-long black hole-neutron star mergers. *Phys. Rev. D* **106**(2), 023,008 (2022). <https://doi.org/10.1103/PhysRevD.106.023008>. arXiv:2111.04621 [astro-ph.HE]
32. R.D. Blandford, R.L. Znajek, Electromagnetic extraction of energy from Kerr black holes. *Mon. Not. Roy. Astron. Soc.* **179**, 433–456 (1977)
33. W. Lu, E. Quataert, Late-time accretion in neutron star mergers: Implications for short gamma-ray bursts and kilonovae. *Mon. Not. Roy. Astron. Soc.* **522**(4), 5848–5861 (2023). <https://doi.org/10.1093/mnras/stad1336>. arXiv:2208.04293 [astro-ph.HE]
34. F. Özel, D. Psaltis, R. Narayan, J.E. McClintock, The Black Hole Mass Distribution in the Galaxy. *Astrophys. J.* **725**(2), 1918–1927 (2010). <https://doi.org/10.1088/0004-637X/725/2/1918>. arXiv:1006.2834 [astro-ph.GA]
35. W.M. Farr, N. Sravan, A. Cantrell, L. Kreidberg, C.D. Bailyn, I. Mandel, V. Kalogera, The Mass Distribution of Stellar-mass Black Holes. *Astrophys. J.* **741**(2), 103 (2011). <https://doi.org/10.1088/0004-637X/741/2/103>. arXiv:1011.1459 [astro-ph.GA]
36. R. Abbott, et al., Population Properties of Compact Objects from the Second LIGO-Virgo Gravitational-Wave Transient Catalog. *Astrophys. J. Lett.* **913**(1), L7 (2021). <https://doi.org/10.3847/2041-8213/abe949>. arXiv:2010.14533 [astro-ph.HE]
37. T. Hinderer, et al., Distinguishing the nature of comparable-mass neutron star binary systems with multimessenger observations: GW170817 case study. *Phys. Rev. D* **100**(6), 06,321 (2019). <https://doi.org/10.1103/PhysRevD.100.063021>. arXiv:1808.03836 [astro-ph.HE]
38. F. Özel, P. Freire, Masses, Radii, and the Equation of State of Neutron Stars. *Ann. Rev. Astron. Astrophys.* **54**, 401–440 (2016). <https://doi.org/10.1146/annurev-astro-081915-023322>. arXiv:1603.02698 [astro-ph.HE]
39. B.P. Abbott, et al., GW190425: Observation of a Compact Binary Coalescence with Total Mass $\sim 3.4M_{\odot}$. *Astrophys. J. Lett.* **892**(1), L3 (2020). <https://doi.org/10.3847/2041-8213/ab75f5>. arXiv:2001.01761 [astro-ph.HE]
40. C.S. Kochanek, Coalescing Binary Neutron Stars. *Astrophys. J.* **398**, 234 (1992). <https://doi.org/10.1086/171851>

41. L. Bildsten, C. Cutler, Tidal Interactions of Inspiring Compact Binaries. *Astrophys. J.* **400**, 175 (1992). <https://doi.org/10.1086/171983>
42. W.E. East, V. Paschalidis, F. Pretorius, Eccentric mergers of black holes with spinning neutron stars. *Astrophys. J. Lett.* **807**(1), L3 (2015). <https://doi.org/10.1088/2041-8205/807/1/L3>. [arXiv:1503.07171](https://arxiv.org/abs/1503.07171) [astro-ph.HE]
43. M. Ruiz, V. Paschalidis, A. Tsokaros, S.L. Shapiro, Black hole-neutron star coalescence: effects of the neutron star spin on jet launching and dynamical ejecta mass. *Phys. Rev. D* **102**(12), 124,077 (2020). <https://doi.org/10.1103/PhysRevD.102.124077>. [arXiv:2011.08863](https://arxiv.org/abs/2011.08863) [astro-ph.HE]
44. F. Foucart, T. Hinderer, S. Nissanke, Remnant baryon mass in neutron star-black hole mergers: Predictions for binary neutron star mimickers and rapidly spinning black holes. *Phys. Rev. D* **98**(8), 081,501 (2018). <https://doi.org/10.1103/PhysRevD.98.081501>. [arXiv:1807.00011](https://arxiv.org/abs/1807.00011) [astro-ph.HE]
45. K. Kawaguchi, K. Kyutoku, M. Shibata, M. Tanaka, Models of Kilonova/macronova Emission From Black Hole–neutron Star Mergers. *Astrophys. J.* **825**(1), 52 (2016). <https://doi.org/10.3847/0004-637X/825/1/52>. [arXiv:1601.07711](https://arxiv.org/abs/1601.07711) [astro-ph.HE]
46. F. Foucart, Black Hole-Neutron Star Mergers: Disk Mass Predictions. *Phys. Rev. D* **86**, 124,007 (2012). <https://doi.org/10.1103/PhysRevD.86.124007>. [arXiv:1207.6304](https://arxiv.org/abs/1207.6304) [astro-ph.HE]
47. C.J. Krüger, F. Foucart, Estimates for Disk and Ejecta Masses Produced in Compact Binary Mergers. *Phys. Rev. D* **101**(10), 103,002 (2020). <https://doi.org/10.1103/PhysRevD.101.103002>. [arXiv:2002.07728](https://arxiv.org/abs/2002.07728) [astro-ph.HE]
48. K. Hayashi, K. Kawaguchi, K. Kiuchi, K. Kyutoku, M. Shibata, Properties of the remnant disk and the dynamical ejecta produced in low-mass black hole-neutron star mergers. *Phys. Rev. D* **103**(4), 043,007 (2021). <https://doi.org/10.1103/PhysRevD.103.043007>. [arXiv:2010.02563](https://arxiv.org/abs/2010.02563) [astro-ph.HE]
49. F. Pannarale, Black hole remnant of black hole-neutron star coalescing binaries. *Phys. Rev. D* **88**(10), 104,025 (2013). <https://doi.org/10.1103/PhysRevD.88.104025>. [arXiv:1208.5869](https://arxiv.org/abs/1208.5869) [gr-qc]
50. F. Pannarale, Black hole remnant of black hole-neutron star coalescing binaries with arbitrary black hole spin. *Phys. Rev. D* **89**(4), 044,045 (2014). <https://doi.org/10.1103/PhysRevD.89.044045>. [arXiv:1311.5931](https://arxiv.org/abs/1311.5931) [gr-qc]
51. K. Kyutoku, H. Okawa, M. Shibata, K. Taniguchi, Gravitational waves from spinning black hole-neutron star binaries: dependence on black hole spins and on neutron star equations of state. *Phys. Rev. D* **84**, 064,018 (2011). <https://doi.org/10.1103/PhysRevD.84.064018>. [arXiv:1108.1189](https://arxiv.org/abs/1108.1189) [astro-ph.HE]
52. F. Pannarale, E. Berti, K. Kyutoku, B.D. Lackey, M. Shibata, Aligned spin neutron star-black hole mergers: a gravitational waveform amplitude model. *Phys. Rev. D* **92**(8), 084,050 (2015). <https://doi.org/10.1103/PhysRevD.92.084050>. [arXiv:1509.00512](https://arxiv.org/abs/1509.00512) [gr-qc]
53. F. Pannarale, E. Berti, K. Kyutoku, B.D. Lackey, M. Shibata, Gravitational-wave cut-off frequencies of tidally disruptive neutron star-black hole binary mergers. *Phys. Rev. D* **92**(8), 081,504 (2015). <https://doi.org/10.1103/PhysRevD.92.081504>. [arXiv:1509.06209](https://arxiv.org/abs/1509.06209) [gr-qc]
54. M. Shibata, K. Uryu, Simulation of merging binary neutron stars in full general relativity: Gamma = two case. *Phys. Rev. D* **61**, 064,001 (2000). <https://doi.org/10.1103/PhysRevD.61.064001>. [arXiv:gr-qc/9911058](https://arxiv.org/abs/gr-qc/9911058) [gr-qc]
55. W. Kluzniak, W.H. Lee, Simulations of binary coalescence of a neutron star and a black hole. *Astrophys. J.* **494**, L53 (1998). <https://doi.org/10.1086/311151>. [arXiv:astro-ph/9712019](https://arxiv.org/abs/astro-ph/9712019) [astro-ph]
56. W.H. Lee, Newtonian hydrodynamics of the coalescence of black holes with neutron stars. 3. Irrotational binaries with a stiff equation of state. *Mon. Not. Roy. Astron. Soc.* **318**, 606 (2000). <https://doi.org/10.1046/j.1365-8711.2000.03870.x>. [arXiv:astro-ph/0007206](https://arxiv.org/abs/astro-ph/0007206) [astro-ph]

57. W.H. Lee, Newtonian hydrodynamics of the coalescence of black holes with neutron stars IV: Irrotational binaries with a soft equation of state. *Mon. Not. Roy. Astron. Soc.* **328**, 583 (2001). <https://doi.org/10.1046/j.1365-8711.2001.04898.x>. [arXiv:astro-ph/0108236](https://arxiv.org/abs/astro-ph/0108236)
58. H.T. Janka, T. Eberl, M. Ruffert, C.L. Fryer, Black hole: Neutron star mergers as central engines of gamma-ray bursts. *Astrophys. J.* **527**, L39 (1999). <https://doi.org/10.1086/312397>. [arXiv:astro-ph/9908290](https://arxiv.org/abs/astro-ph/9908290) [astro-ph]
59. S. Rosswog, R. Speith, G.A. Wynn, Accretion dynamics in neutron star black hole binaries. *Mon. Not. Roy. Astron. Soc.* **351**, 1121 (2004). <https://doi.org/10.1111/j.1365-2966.2004.07865.x>. [arXiv:astro-ph/0403500](https://arxiv.org/abs/astro-ph/0403500) [astro-ph]
60. S. Rosswog, On the viability of neutron star black hole binaries as central engines of gamma-ray bursts (2005). [arXiv:astro-ph/0505007](https://arxiv.org/abs/astro-ph/0505007) [astro-ph]
61. M. Ruffert, H.T. Janka, Polytropic neutron star - black hole merger simulations with a Paczyński-Wiita potential. *Astron. Astrophys.* **514**, A66 (2010). <https://doi.org/10.1051/0004-6361/200912738>. [arXiv:0906.3998](https://arxiv.org/abs/0906.3998) [astro-ph.HE]
62. B. Paczyński, P.J. Wiita, Thick Accretion Disks and Supercritical Luminosities. *Astron. Astrophys.* **88**, 23 (1980)
63. I.V. Artemova, G. Bjoernsson, I.D. Novikov, Modified Newtonian Potentials for the Description of Relativistic Effects in Accretion Disks around Black Holes. *Astrophys. J.* **461**, 565 (1996). <https://doi.org/10.1086/177084>
64. T.W. Baumgarte, S.L. Shapiro, *Numerical Relativity: Solving Einstein's Equations on the Computer* (2010)
65. H.P. Pfeiffer, D.A. Brown, L.E. Kidder, L. Lindblom, G. Lovelace, M.A. Scheel, Reducing orbital eccentricity in binary black hole simulations. *Class. Quant. Grav.* **24**, S59–S82 (2007). <https://doi.org/10.1088/0264-9381/24/12/S06>. [arXiv:gr-qc/0702106](https://arxiv.org/abs/gr-qc/0702106)
66. M.A. Miller, General relativistic initial data for the binary black hole / neutron star system in quasicircular orbit (2001). [arXiv:gr-qc/0106017](https://arxiv.org/abs/gr-qc/0106017)
67. P. Grandclement, Accurate and realistic initial data for black hole-neutron star binaries. *Phys. Rev. D* **74**, 124,002 (2006). <https://doi.org/10.1103/PhysRevD.74.124002>. [Erratum: *Phys.Rev.D* 75, 129903 (2007)]. [arXiv:gr-qc/0609044](https://arxiv.org/abs/gr-qc/0609044)
68. K. Taniguchi, T.W. Baumgarte, J.A. Faber, S.L. Shapiro, Quasiequilibrium sequences of black-hole-neutron-star binaries in general relativity. *Phys. Rev. D* **74**, 041,502 (2006). <https://doi.org/10.1103/PhysRevD.74.041502>. [arXiv:gr-qc/0609053](https://arxiv.org/abs/gr-qc/0609053)
69. W. Tichy, The initial value problem as it relates to numerical relativity. *Rept. Prog. Phys.* **80**(2), 026,901 (2017). <https://doi.org/10.1088/1361-6633/80/2/026901>. [arXiv:1610.03805](https://arxiv.org/abs/1610.03805) [gr-qc]
70. M.D. Duez, Y. Zlochower, Numerical Relativity of Compact Binaries in the 21st Century. *Rept. Prog. Phys.* **82**(1), 016,902 (2019). <https://doi.org/10.1088/1361-6633/aadb16>. [arXiv:1808.06011](https://arxiv.org/abs/1808.06011) [gr-qc]
71. F. Löffler, L. Rezzolla, M. Ansorg, Numerical evolutions of a black hole-neutron star system in full general relativity: Head-on collision. *Phys. Rev. D* **74**, 104,018 (2006). <https://doi.org/10.1103/PhysRevD.74.104018>. URL <https://link.aps.org/doi/10.1103/PhysRevD.74.104018>
72. M. Shibata, K. Uryu, Merger of black hole-neutron star binaries in full general relativity. *Class. Quant. Grav.* **24**, S125–S138 (2007). <https://doi.org/10.1088/0264-9381/24/12/S09>. [arXiv:astro-ph/0611522](https://arxiv.org/abs/astro-ph/0611522) [astro-ph]
73. Z.B. Etienne, J.A. Faber, Y.T. Liu, S.L. Shapiro, K. Taniguchi, T.W. Baumgarte, Fully General Relativistic Simulations of Black Hole-Neutron Star Mergers. *Phys. Rev.* **D77**, 084,002 (2008). <https://doi.org/10.1103/PhysRevD.77.084002>. [arXiv:0712.2460](https://arxiv.org/abs/0712.2460) [astro-ph]
74. M.D. Duez, F. Foucart, L.E. Kidder, H.P. Pfeiffer, M.A. Scheel, S.A. Teukolsky, Evolving black hole-neutron star binaries in general relativity using pseudospectral and finite difference methods. *Phys. Rev.* **D78**, 104,015 (2008). <https://doi.org/10.1103/PhysRevD.78.104015>. [arXiv:0809.0002](https://arxiv.org/abs/0809.0002) [gr-qc]

75. S. Chawla, M. Anderson, M. Besselman, L. Lehner, S.L. Liebling, P.M. Motl, D. Neilsen, Mergers of Magnetized Neutron Stars with Spinning Black Holes: Disruption, Accretion and Fallback. *Phys. Rev. Lett.* **105**, 111,101 (2010). <https://doi.org/10.1103/PhysRevLett.105.111101>. [arXiv:1006.2839](https://arxiv.org/abs/1006.2839) [gr-qc]
76. J.S. Read, B.D. Lackey, B.J. Owen, J.L. Friedman, Constraints on a phenomenologically parameterized neutron-star equation of state. *Phys. Rev.* **D79**, 124,032 (2009). <https://doi.org/10.1103/PhysRevD.79.124032>. [arXiv:0812.2163](https://arxiv.org/abs/0812.2163) [astro-ph]
77. M.F. O’Boyle, C. Markakis, N. Stergioulas, J.S. Read, Parametrized equation of state for neutron star matter with continuous sound speed. *Phys. Rev. D* **102**(8), 083,027 (2020). <https://doi.org/10.1103/PhysRevD.102.083027>. [arXiv:2008.03342](https://arxiv.org/abs/2008.03342) [astro-ph.HE]
78. L. Lindblom, Spectral Representations of Neutron-Star Equations of State. *Phys. Rev. D* **82**, 103,011 (2010). <https://doi.org/10.1103/PhysRevD.82.103011>. [arXiv:1009.0738](https://arxiv.org/abs/1009.0738) [astro-ph.HE]
79. F. Foucart, M.D. Duez, A. Gudinas, F. Hebert, L.E. Kidder, H.P. Pfeiffer, M.A. Scheel, Smooth Equations of State for High-Accuracy Simulations of Neutron Star Binaries. *Phys. Rev. D* **100**(10), 104,048 (2019). <https://doi.org/10.1103/PhysRevD.100.104048>. [arXiv:1908.05277](https://arxiv.org/abs/1908.05277) [gr-qc]
80. B.D. Metzger, G. Martínez-Pinedo, S. Darbha, E. Quataert, A. Arcones, D. Kasen, R. Thomas, P. Nugent, I.V. Panov, N.T. Zinner, Electromagnetic counterparts of compact object mergers powered by the radioactive decay of r-process nuclei. *Mon. Not. Roy. Astron. Soc.* **406**(4), 2650–2662 (2010). <https://doi.org/10.1111/j.1365-2966.2010.16864.x>. [arXiv:1001.5029](https://arxiv.org/abs/1001.5029) [astro-ph.HE]
81. S. Rosswog, O. Korobkin, A. Arcones, F.K. Thielemann, T. Piran, The long-term evolution of neutron star merger remnants – I. The impact of r-process nucleosynthesis. *Mon. Not. Roy. Astron. Soc.* **439**(1), 744–756 (2014). <https://doi.org/10.1093/mnras/stt2502>. [arXiv:1307.2939](https://arxiv.org/abs/1307.2939) [astro-ph.HE]
82. D. Desai, B.D. Metzger, F. Foucart, Imprints of r-process heating on fall-back accretion: distinguishing black hole–neutron star from double neutron star mergers. *Mon. Not. Roy. Astron. Soc.* **485**(3), 4404–4412 (2019). <https://doi.org/10.1093/mnras/stz644>. [arXiv:1812.04641](https://arxiv.org/abs/1812.04641) [astro-ph.HE]
83. F. Magistrelli, S. Bernuzzi, A. Perego, D. Radice, Elements formation in radiation-hydrodynamics simulations of kilonovae (2024). [arXiv:2403.13883](https://arxiv.org/abs/2403.13883) [astro-ph.HE]
84. M.B. Deaton, M.D. Duez, F. Foucart, E. O’Connor, C.D. Ott, L.E. Kidder, C.D. Muhlberger, M.A. Scheel, B. Szilagyi, Black Hole-Neutron Star Mergers with a Hot Nuclear Equation of State: Outflow and Neutrino-Cooled Disk for a Low-Mass, High-Spin Case. *Astrophys. J.* **776**, 47 (2013). <https://doi.org/10.1088/0004-637X/776/1/47>. [arXiv:1304.3384](https://arxiv.org/abs/1304.3384) [astro-ph.HE]
85. W. Brege, M.D. Duez, F. Foucart, M.B. Deaton, J. Caro, D.A. Hemberger, L.E. Kidder, E. O’Connor, H.P. Pfeiffer, M.A. Scheel, Black hole-neutron star mergers using a survey of finite-temperature equations of state. *Phys. Rev. D* **98**(6), 063,009 (2018). <https://doi.org/10.1103/PhysRevD.98.063009>. [arXiv:1804.09823](https://arxiv.org/abs/1804.09823) [gr-qc]
86. K.S. Thorne, Relativistic radiative transfer: moment formalisms. *Mon. Not. Roy. Astron. Soc.* **194**(2), 439–473 (1981). <https://doi.org/10.1093/mnras/194.2.439>
87. M. Shibata, K. Kiuchi, Y.i. Sekiguchi, Y. Suwa, Truncated Moment Formalism for Radiation Hydrodynamics in Numerical Relativity. *Prog. Theor. Phys.* **125**, 1255–1287 (2011). <https://doi.org/10.1143/PTP.125.1255>. [arXiv:1104.3937](https://arxiv.org/abs/1104.3937) [astro-ph.HE]
88. F. Foucart, E. O’Connor, L. Roberts, M.D. Duez, R. Haas, L.E. Kidder, C.D. Ott, H.P. Pfeiffer, M.A. Scheel, B. Szilagyi, Post-merger evolution of a neutron star-black hole binary with neutrino transport. *Phys. Rev. D* **91**(12), 124,021 (2015). <https://doi.org/10.1103/PhysRevD.91.124021>. [arXiv:1502.04146](https://arxiv.org/abs/1502.04146) [astro-ph.HE]
89. K. Kyutoku, K. Kiuchi, Y. Sekiguchi, M. Shibata, K. Taniguchi, Neutrino transport in black hole-neutron star binaries: neutrino emission and dynamical mass ejection. *Phys. Rev. D* **97**(2), 023,009 (2018). <https://doi.org/10.1103/PhysRevD.97.023009>. [arXiv:1710.00827](https://arxiv.org/abs/1710.00827) [astro-ph.HE]

90. J.M. Miller, B.R. Ryan, J.C. Dolence, *vhlight*: Radiation GRMHD for Neutrino-Driven Accretion Flows. *Astrophys. J. Suppl.* **241**(2), 30 (2019). <https://doi.org/10.3847/1538-4365/ab09fc>. [arXiv:1903.09273](https://arxiv.org/abs/1903.09273) [astro-ph.IM]
91. F. Foucart, M.D. Duez, F. Hebert, L.E. Kidder, P. Kovarik, H.P. Pfeiffer, M.A. Scheel, Implementation of Monte Carlo Transport in the General Relativistic SpEC Code. *Astrophys. J.* **920**(2), 82 (2021). <https://doi.org/10.3847/1538-4357/ac1737>. [arXiv:2103.16588](https://arxiv.org/abs/2103.16588) [astro-ph.HE]
92. J.M. Miller, B.R. Ryan, J.C. Dolence, A. Burrows, C.J. Fontes, C.L. Fryer, O. Korobkin, J. Lippuner, M.R. Mumpower, R.T. Wollaeger, Full Transport Model of GW170817-Like Disk Produces a Blue Kilonova. *Phys. Rev. D* **100**(2), 023,008 (2019). <https://doi.org/10.1103/PhysRevD.100.023008>. [arXiv:1905.07477](https://arxiv.org/abs/1905.07477) [astro-ph.HE]
93. Y. Masada, T. Sano, Axisymmetric Magnetorotational Instability in Viscous Accretion Disks. *Astrophys. J.* **689**, 1234 (2008). <https://doi.org/10.1086/592601>. [arXiv:0808.2338](https://arxiv.org/abs/0808.2338) [astro-ph]
94. J. Guilet, E. Mueller, H.T. Janka, Neutrino viscosity and drag: impact on the magnetorotational instability in protoneutron stars. *Mon. Not. Roy. Astron. Soc.* **447**, 3992 (2015). <https://doi.org/10.1093/mnras/stu2550>. [arXiv:1410.1874](https://arxiv.org/abs/1410.1874) [astro-ph.HE]
95. K. Kiuchi, Y. Sekiguchi, K. Kyutoku, M. Shibata, K. Taniguchi, T. Wada, High resolution magnetohydrodynamic simulation of black hole-neutron star merger: Mass ejection and short gamma ray bursts. *Phys. Rev. D* **92**(6), 064,034 (2015). <https://doi.org/10.1103/PhysRevD.92.064034>. [arXiv:1506.06811](https://arxiv.org/abs/1506.06811) [astro-ph.HE]
96. A. Malkus, G.C. McLaughlin, R. Surman, Symmetric and Standard Matter-Neutrino Resonances Above Merging Compact Objects. *Phys. Rev. D* **93**(4), 045,021 (2016). <https://doi.org/10.1103/PhysRevD.93.045021>. [arXiv:1507.00946](https://arxiv.org/abs/1507.00946) [hep-ph]
97. X. Li, D.M. Siegel, Neutrino Fast Flavor Conversions in Neutron-Star Postmerger Accretion Disks. *Phys. Rev. Lett.* **126**(25), 251,101 (2021). <https://doi.org/10.1103/PhysRevLett.126.251101>. [arXiv:2103.02616](https://arxiv.org/abs/2103.02616) [astro-ph.HE]
98. F. Foucart, Neutrino transport in general relativistic neutron star merger simulations. *Living Reviews in Computational Astrophysics* **9**(1), 1 (2023). <https://doi.org/10.1007/s41115-023-00016-y>. [arXiv:2209.02538](https://arxiv.org/abs/2209.02538) [astro-ph.HE]
99. E.E. Flanagan, T. Hinderer, Constraining neutron star tidal Love numbers with gravitational wave detectors. *Phys. Rev. D* **77**, 021,502 (2008). <https://doi.org/10.1103/PhysRevD.77.021502>. [arXiv:0709.1915](https://arxiv.org/abs/0709.1915) [astro-ph]
100. M. Shibata, K. Kyutoku, T. Yamamoto, K. Taniguchi, Gravitational waves from black hole-neutron star binaries I: Classification of waveforms. *Phys. Rev. D* **79**, 044,030 (2009). <https://doi.org/10.1103/PhysRevD.79.044030>. [Erratum: *Phys.Rev.D* **85**, 127502 (2012)]. [arXiv:0902.0416](https://arxiv.org/abs/0902.0416) [gr-qc]
101. F. Foucart, L. Buchman, M.D. Duez, M. Grudich, L.E. Kidder, I. MacDonald, A. Mroue, H.P. Pfeiffer, M.A. Scheel, B. Szilagy, First direct comparison of nondisrupting neutron star-black hole and binary black hole merger simulations. *Phys. Rev. D* **88**(6), 064,017 (2013). <https://doi.org/10.1103/PhysRevD.88.064017>. [arXiv:1307.7685](https://arxiv.org/abs/1307.7685) [gr-qc]
102. K. Kyutoku, M. Shibata, K. Taniguchi, Gravitational waves from nonspinning black hole-neutron star binaries: dependence on equations of state. *Phys. Rev. D* **82**, 044,049 (2010). <https://doi.org/10.1103/PhysRevD.82.044049>. [Erratum: *Phys.Rev.D* **84**, 049902 (2011)]. [arXiv:1008.1460](https://arxiv.org/abs/1008.1460) [astro-ph.HE]
103. B.D. Lackey, K. Kyutoku, M. Shibata, P.R. Brady, J.L. Friedman, Extracting equation of state parameters from black hole-neutron star mergers: aligned-spin black holes and a preliminary waveform model. *Phys. Rev. D* **89**(4), 043,009 (2014). <https://doi.org/10.1103/PhysRevD.89.043009>. [arXiv:1303.6298](https://arxiv.org/abs/1303.6298) [gr-qc]
104. J.E. Thompson, E. Fauchon-Jones, S. Khan, E. Nitoglia, F. Pannarale, T. Dietrich, M. Hannam, Modeling the gravitational wave signature of neutron star black hole coalescences. *Phys. Rev. D* **101**(12), 124,059 (2020). <https://doi.org/10.1103/PhysRevD.101.124059>. [arXiv:2002.08383](https://arxiv.org/abs/2002.08383) [gr-qc]
105. A. Matas, et al., Aligned-spin neutron-star-black-hole waveform model based on the effective-one-body approach and numerical-relativity simulations. *Phys. Rev. D*

- 102**(4), 043,023 (2020). <https://doi.org/10.1103/PhysRevD.102.043023>. [arXiv:2004.10001](https://arxiv.org/abs/2004.10001) [gr-qc]
106. K. Chakravarti, et al., Systematic effects from black hole-neutron star waveform model uncertainties on the neutron star equation of state. *Phys. Rev. D* **99**(2), 024,049 (2019). <https://doi.org/10.1103/PhysRevD.99.024049>. [arXiv:1809.04349](https://arxiv.org/abs/1809.04349) [gr-qc]
 107. Y. Huang, C.J. Haster, S. Vitale, V. Varma, F. Foucart, S. Biscoveanu, Statistical and systematic uncertainties in extracting the source properties of neutron star - black hole binaries with gravitational waves. *Phys. Rev. D* **103**(8), 083,001 (2021). <https://doi.org/10.1103/PhysRevD.103.083001>. [arXiv:2005.11850](https://arxiv.org/abs/2005.11850) [gr-qc]
 108. P. Goldreich, W.H. Julian, Pulsar Electrodynamics. *Astrophys. J.* **157**, 869 (1969). <https://doi.org/10.1086/150119>
 109. V. Paschalidis, Z.B. Etienne, S.L. Shapiro, General relativistic simulations of binary black hole-neutron stars: Precursor electromagnetic signals. *Phys. Rev.* **D88**(2), 021,504 (2013). <https://doi.org/10.1103/PhysRevD.88.021504>. [arXiv:1304.1805](https://arxiv.org/abs/1304.1805) [astro-ph.HE]
 110. S.T. McWilliams, J. Levin, Electromagnetic extraction of energy from black hole-neutron star binaries. *Astrophys. J.* **742**, 90 (2011). <https://doi.org/10.1088/0004-637X/742/2/90>. [arXiv:1101.1969](https://arxiv.org/abs/1101.1969) [astro-ph.HE]
 111. V. Paschalidis, S.L. Shapiro, A new scheme for matching general relativistic ideal magnetohydrodynamics to its force-free limit. *Phys. Rev. D* **88**(10), 104,031 (2013). <https://doi.org/10.1103/PhysRevD.88.104031>. [arXiv:1310.3274](https://arxiv.org/abs/1310.3274) [astro-ph.HE]
 112. W.E. East, L. Lehner, S.L. Liebling, C. Palenzuela, Multimessenger Signals from Black Hole–Neutron Star Mergers without Significant Tidal Disruption. *Astrophys. J. Lett.* **912**(1), L18 (2021). <https://doi.org/10.3847/2041-8213/2041-8213/abf566>. [arXiv:2101.12214](https://arxiv.org/abs/2101.12214) [astro-ph.HE]
 113. E.R. Most, A.A. Philippov, Electromagnetic Precursors to Black Hole–Neutron Star Gravitational Wave Events: Flares and Reconnection-powered Fast Radio Transients from the Late Inspiral. *Astrophys. J. Lett.* **956**(2), L33 (2023). <https://doi.org/10.3847/2041-8213/acfdac>. [arXiv:2309.04271](https://arxiv.org/abs/2309.04271) [astro-ph.HE]
 114. C. Palenzuela, Modeling magnetized neutron stars using resistive MHD. *Mon. Not. Roy. Astron. Soc.* **431**, 1853–1865 (2013). <https://doi.org/10.1093/mnras/stt311>. [arXiv:1212.0130](https://arxiv.org/abs/1212.0130) [astro-ph.HE]
 115. E.R. Most, A.A. Philippov, Electromagnetic precursor flares from the late inspiral of neutron star binaries. *Mon. Not. Roy. Astron. Soc.* **515**(2), 2710–2724 (2022). <https://doi.org/10.1093/mnras/stac1909>. [arXiv:2205.09643](https://arxiv.org/abs/2205.09643) [astro-ph.HE]
 116. M.D. Duez, F. Foucart, L.E. Kidder, C.D. Ott, S.A. Teukolsky, Equation of state effects in black hole-neutron star mergers. *Class. Quant. Grav.* **27**, 114,106 (2010). <https://doi.org/10.1088/0264-9381/27/11/114106>. [arXiv:0912.3528](https://arxiv.org/abs/0912.3528) [astro-ph.HE]
 117. W.E. East, F. Pretorius, B.C. Stephens, Eccentric black hole-neutron star mergers: effects of black hole spin and equation of state. *Phys. Rev.* **D85**, 124,009 (2012). <https://doi.org/10.1103/PhysRevD.85.124009>. [arXiv:1111.3055](https://arxiv.org/abs/1111.3055) [astro-ph.HE]
 118. Z.B. Etienne, Y.T. Liu, S.L. Shapiro, T.W. Baumgarte, General relativistic simulations of black-hole-neutron-star mergers: Effects of black-hole spin. *Phys. Rev.* **D79**, 044,024 (2009). <https://doi.org/10.1103/PhysRevD.79.044024>. [arXiv:0812.2245](https://arxiv.org/abs/0812.2245) [astro-ph]
 119. G. Lovelace, M.D. Duez, F. Foucart, L.E. Kidder, H.P. Pfeiffer, M.A. Scheel, B. Szilágyi, Massive disc formation in the tidal disruption of a neutron star by a nearly extremal black hole. *Class. Quant. Grav.* **30**, 135,004 (2013). <https://doi.org/10.1088/0264-9381/30/13/135004>. [arXiv:1302.6297](https://arxiv.org/abs/1302.6297) [gr-qc]
 120. F. Foucart, M.D. Duez, L.E. Kidder, M.A. Scheel, B. Szilágyi, S.A. Teukolsky, Black hole-neutron star mergers for 10 solar mass black holes. *Phys. Rev. D* **85**, 044,015 (2012). <https://doi.org/10.1103/PhysRevD.85.044015>. [arXiv:1111.1677](https://arxiv.org/abs/1111.1677) [gr-qc]
 121. K. Kyutoku, K. Ioka, H. Okawa, M. Shibata, K. Taniguchi, Dynamical mass ejection from black hole-neutron star binaries. *Phys. Rev. D* **92**, 044,028 (2015). <https://doi.org/10.1103/PhysRevD.92.044028>. [arXiv:1502.05402](https://arxiv.org/abs/1502.05402) [astro-ph.HE]

122. F. Foucart, M.D. Duez, L.E. Kidder, S.A. Teukolsky, Black hole-neutron star mergers: effects of the orientation of the black hole spin. *Phys. Rev.* **D83**, 024,005 (2011). <https://doi.org/10.1103/PhysRevD.83.024005>. [arXiv:1007.4203](https://arxiv.org/abs/1007.4203) [astro-ph.HE]
123. K. Kawaguchi, K. Kyutoku, H. Nakano, H. Okawa, M. Shibata, K. Taniguchi, Black hole-neutron star binary merger: Dependence on black hole spin orientation and equation of state. *Phys. Rev.* **D92**(2), 024,014 (2015). <https://doi.org/10.1103/PhysRevD.92.024014>. [arXiv:1506.05473](https://arxiv.org/abs/1506.05473) [astro-ph.HE]
124. N. Stone, A. Loeb, E. Berger, Pulsations in Short GRBs from Black Hole-Neutron Star Mergers. *Phys. Rev. D* **87**, 084,053 (2013). <https://doi.org/10.1103/PhysRevD.87.084053>. [arXiv:1209.4097](https://arxiv.org/abs/1209.4097) [astro-ph.HE]
125. S. Rosswog, fallback accretion in the aftermath of a compact binary merger. *Mon. Not. Roy. Astron. Soc.* **376**, L48–L51 (2007). <https://doi.org/10.1111/j.1745-3933.2007.00284.x>. [arXiv:astro-ph/0611440](https://arxiv.org/abs/astro-ph/0611440)
126. M.J. Rees, Tidal disruption of stars by black holes of 10^6 - 10^8 solar masses in nearby galaxies. *Nature* **333**(6173), 523–528 (1988). <https://doi.org/10.1038/333523a0>
127. E.S. Phinney, in *The Center of the Galaxy*, vol. 136, ed. by M. Morris (1989), p. 543
128. G. Lodato, A.R. King, J.E. Pringle, Stellar disruption by a supermassive black hole: is the light curve really proportional to $t^{-5/3}$? *Mon. Not. Roy. Astron. Soc.* **392**, 332 (2009). <https://doi.org/10.1111/j.1365-2966.2008.14049.x>. [arXiv:0810.1288](https://arxiv.org/abs/0810.1288) [astro-ph]
129. R. Fernández, E. Quataert, J. Schwab, D. Kasen, S. Rosswog, The interplay of disc wind and dynamical ejecta in the aftermath of neutron star–black hole mergers. *Mon. Not. Roy. Astron. Soc.* **449**(1), 390–402 (2015). <https://doi.org/10.1093/mnras/stv238>. [arXiv:1412.5588](https://arxiv.org/abs/1412.5588) [astro-ph.HE]
130. S. De, D.M. Siegel, Igniting Weak Interactions in Neutron Star Postmerger Accretion Disks. *Astrophys. J.* **921**(1), 94 (2021). <https://doi.org/10.3847/1538-4357/ac110b>. [arXiv:2011.07176](https://arxiv.org/abs/2011.07176) [astro-ph.HE]
131. A.M. Beloborodov, Nuclear composition of gamma-ray burst fireballs. *Astrophys. J.* **588**, 931–944 (2003). <https://doi.org/10.1086/374217>. [arXiv:astro-ph/0210522](https://arxiv.org/abs/astro-ph/0210522)
132. D.M. Siegel, B.D. Metzger, Three-dimensional GRMHD simulations of neutrino-cooled accretion disks from neutron star mergers. *Astrophys. J.* **858**(1), 52 (2018). <https://doi.org/10.3847/1538-4357/aabaec>. [arXiv:1711.00868](https://arxiv.org/abs/1711.00868) [astro-ph.HE]
133. R. Narayan, I.V. Igumenshchev, M.A. Abramowicz, Magnetically arrested disk: an energetically efficient accretion flow. *Publ. Astron. Soc. Jap.* **55**, L69 (2003). <https://doi.org/10.1093/pasj/55.6.L69>. [arXiv:astro-ph/0305029](https://arxiv.org/abs/astro-ph/0305029)
134. A. Tchekhovskoy, R. Narayan, J.C. McKinney, Efficient generation of jets from magnetically arrested accretion on a rapidly spinning black hole. *Mon. Not. Roy. Astron. Soc.* **418**(1), L79–L83 (2011). <https://doi.org/10.1111/j.1745-3933.2011.01147.x>. [arXiv:1108.0412](https://arxiv.org/abs/1108.0412) [astro-ph.HE]
135. M.R. Izquierdo, M. Bezares, S. Liebling, C. Palenzuela, Large Eddy Simulations of Magnetized Mergers of Black Holes and Neutron Stars (2024). [arXiv:2403.09770](https://arxiv.org/abs/2403.09770) [astro-ph.HE]
136. S.A. Balbus, J.F. Hawley, Instability, turbulence, and enhanced transport in accretion disks. *Reviews of Modern Physics* **70**(1), 1–53 (1998). <https://doi.org/10.1103/RevModPhys.70.1>
137. Z.B. Etienne, Y.T. Liu, V. Paschalidis, S.L. Shapiro, General relativistic simulations of black hole-neutron star mergers: Effects of magnetic fields. *Phys. Rev.* **D85**, 064,029 (2012). <https://doi.org/10.1103/PhysRevD.85.064029>. [arXiv:1112.0568](https://arxiv.org/abs/1112.0568) [astro-ph.HE]
138. Z.B. Etienne, V. Paschalidis, S.L. Shapiro, General-relativistic simulations of black-hole-neutron-star mergers: Effects of tilted magnetic fields. *Phys. Rev. D.* **86**(8), 084026 (2012). <https://doi.org/10.1103/PhysRevD.86.084026>. [arXiv:1209.1632](https://arxiv.org/abs/1209.1632) [astro-ph.HE]
139. E.R. Most, L.J. Papenfort, S.D. Tootle, L. Rezzolla, On accretion discs formed in MHD simulations of black hole–neutron star mergers with accurate microphysics. *Mon. Not.*

- Roy. Astron. Soc. **506**(3), 3511–3526 (2021). <https://doi.org/10.1093/mnras/stab1824>. [arXiv:2106.06391](https://arxiv.org/abs/2106.06391) [astro-ph.HE]
140. K. Beckwith, J.F. Hawley, J.H. Krolik, The Influence of Magnetic Field Geometry on the Evolution of Black Hole Accretion Flows: Similar Disks, Drastically Different Jets. *Astrophys. J.* **678**, 1180 (2008). <https://doi.org/10.1086/533492>. [arXiv:0709.3833](https://arxiv.org/abs/0709.3833) [astro-ph]
 141. V. Paschalidis, M. Ruiz, S.L. Shapiro, Relativistic Simulations of Black Hole–neutron Star Coalescence: the jet Emerges. *Astrophys. J. Lett.* **806**(1), L14 (2015). <https://doi.org/10.1088/2041-8205/806/1/L14>. [arXiv:1410.7392](https://arxiv.org/abs/1410.7392) [astro-ph.HE]
 142. M. Ruiz, S.L. Shapiro, A. Tsokaros, Jet launching from binary black hole-neutron star mergers: Dependence on black hole spin, binary mass ratio and magnetic field orientation. *Phys. Rev. D* **98**(12), 123,017 (2018). <https://doi.org/10.1103/PhysRevD.98.123017>. [arXiv:1810.08618](https://arxiv.org/abs/1810.08618) [astro-ph.HE]
 143. O. Gottlieb, et al., Large-scale Evolution of Seconds-long Relativistic Jets from Black Hole–Neutron Star Mergers. *Astrophys. J. Lett.* **954**(1), L21 (2023). <https://doi.org/10.3847/2041-8213/aceeff>. [arXiv:2306.14947](https://arxiv.org/abs/2306.14947) [astro-ph.HE]
 144. H.K. Moffatt, *Magnetic field generation in electrically conducting fluids* (1978)
 145. J.D. Hogg, C. Reynolds, The influence of accretion disk thickness on the large-scale magnetic dynamo. *Astrophys. J.* **861**(1), 24 (2018). <https://doi.org/10.3847/1538-4357/aac439>. [arXiv:1805.05372](https://arxiv.org/abs/1805.05372) [astro-ph.HE]
 146. M.T.P. Liska, A. Tchekhovskoy, E. Quataert, Large-Scale Poloidal Magnetic Field Dynamo Leads to Powerful Jets in GRMHD Simulations of Black Hole Accretion with Toroidal Field. *Mon. Not. Roy. Astron. Soc.* **494**(3), 3656–3662 (2020). <https://doi.org/10.1093/mnras/staa955>. [arXiv:1809.04608](https://arxiv.org/abs/1809.04608) [astro-ph.HE]
 147. I.M. Christie, A. Lalakos, A. Tchekhovskoy, R. Fernández, F. Foucart, E. Quataert, D. Kasen, The Role of Magnetic Field Geometry in the Evolution of Neutron Star Merger Accretion Discs. *Mon. Not. Roy. Astron. Soc.* **490**(4), 4811–4825 (2019). <https://doi.org/10.1093/mnras/stz2552>. [arXiv:1907.02079](https://arxiv.org/abs/1907.02079) [astro-ph.HE]
 148. K. Hayashi, K. Kiuchi, K. Kyutoku, Y. Sekiguchi, M. Shibata, General-relativistic neutrino-radiation magnetohydrodynamics simulation of seconds-long black hole-neutron star mergers: Dependence on the initial magnetic field strength, configuration, and neutron-star equation of state. *Phys. Rev. D* **107**(12), 123,001 (2023). <https://doi.org/10.1103/PhysRevD.107.123001>. [arXiv:2211.07158](https://arxiv.org/abs/2211.07158) [astro-ph.HE]
 149. O. Gottlieb, B.D. Metzger, E. Quataert, D. Issa, T. Martineau, F. Foucart, M.D. Duez, L.E. Kidder, H.P. Pfeiffer, M.A. Scheel, A Unified Picture of Short and Long Gamma-Ray Bursts from Compact Binary Mergers. *Astrophys. J. Lett.* **958**(2), L33 (2023). <https://doi.org/10.3847/2041-8213/ad096e>. [arXiv:2309.00038](https://arxiv.org/abs/2309.00038) [astro-ph.HE]
 150. F.H. Nouri, et al., Evolution of the Magnetized, Neutrino-Cooled Accretion Disk in the Aftermath of a Black Hole Neutron Star Binary Merger. *Phys. Rev. D* **97**(8), 083,014 (2018). <https://doi.org/10.1103/PhysRevD.97.083014>. [arXiv:1710.07423](https://arxiv.org/abs/1710.07423) [astro-ph.HE]
 151. I. Zalamea, A.M. Beloborodov, Neutrino heating near hyper-accreting black holes. *Mon. Not. Roy. Astron. Soc.* **410**(4), 2302–2308 (2011). <https://doi.org/10.1111/j.1365-2966.2010.17600.x>. [arXiv:1003.0710](https://arxiv.org/abs/1003.0710) [astro-ph.HE]
 152. R. Popham, S.E. Woosley, C. Fryer, Hyperaccreting black holes and gamma-ray bursts. *Astrophys. J.* **518**, 356–374 (1999). <https://doi.org/10.1086/307259>. [arXiv:astro-ph/9807028](https://arxiv.org/abs/astro-ph/9807028)
 153. O. Just, M. Obergaulinger, H.T. Janka, A. Bauswein, N. Schwarz, Neutron-star merger ejecta as obstacles to neutrino-powered jets of gamma-ray bursts. *Astrophys. J.* **816**(2), L30 (2016). <https://doi.org/10.3847/2041-8205/816/2/L30>. [arXiv:1510.04288](https://arxiv.org/abs/1510.04288) [astro-ph.HE]
 154. M.V. Barkov, A.S. Pozanenko, Model of extended emission of short Gamma-ray Bursts. *Mon. Not. Roy. Astron. Soc.* **417**, 2161 (2011). <https://doi.org/10.1111/j.1365-2966.2011.19398.x>. [arXiv:1103.4246](https://arxiv.org/abs/1103.4246) [astro-ph.HE]

155. S. Fujibayashi, Y. Sekiguchi, K. Kiuchi, M. Shibata, Properties of Neutrino-driven Ejecta from the Remnant of a Binary Neutron Star Merger: Pure Radiation Hydrodynamics Case. *Astrophys. J.* **846**(2), 114 (2017). <https://doi.org/10.3847/1538-4357/aa8039>. [arXiv:1703.10191](https://arxiv.org/abs/1703.10191) [astro-ph.HE]
156. J.M. Lattimer, D.N. Schramm, The tidal disruption of neutron stars by black holes in close binaries. *Astrophys. J.* **210**, 549–567 (1976). <https://doi.org/10.1086/154860>
157. L.X. Li, B. Paczynski, Transient events from neutron star mergers. *Astrophys. J. Lett.* **507**, L59 (1998). <https://doi.org/10.1086/311680>. [arXiv:astro-ph/9807272](https://arxiv.org/abs/astro-ph/9807272)
158. J. Barnes, D. Kasen, Effect of a High Opacity on the Light Curves of Radioactively Powered Transients from Compact Object Mergers. *Astrophys. J.* **775**, 18 (2013). <https://doi.org/10.1088/0004-637X/775/1/18>. [arXiv:1303.5787](https://arxiv.org/abs/1303.5787) [astro-ph.HE]
159. D. Kasen, N.R. Badnell, J. Barnes, Opacities and Spectra of the *r*-process Ejecta from Neutron Star Mergers. *Astrophys. J.* **774**, 25 (2013). <https://doi.org/10.1088/0004-637X/774/1/25>. [arXiv:1303.5788](https://arxiv.org/abs/1303.5788) [astro-ph.HE]
160. D. Kasen, B. Metzger, J. Barnes, E. Quataert, E. Ramirez-Ruiz, Origin of the heavy elements in binary neutron-star mergers from a gravitational wave event. *Nature* **551**, 80 (2017). <https://doi.org/10.1038/nature24453>. [arXiv:1710.05463](https://arxiv.org/abs/1710.05463) [astro-ph.HE]
161. S. Wanajo, Y. Sekiguchi, N. Nishimura, K. Kiuchi, K. Kyutoku, M. Shibata, Production of All the *r*-process Nuclides in the Dynamical Ejecta of Neutron Star Mergers. *Astrophys. J. Lett.* **789**(2), L39 (2014). <https://doi.org/10.1088/2041-8205/789/2/L39>. [arXiv:1402.7317](https://arxiv.org/abs/1402.7317) [astro-ph.SR]
162. J. Lippuner, L.F. Roberts, *r*-Process Lanthanide Production and Heating Rates in Kilonovae. *Astrophys. J.* **815**(2), 82 (2015). <https://doi.org/10.1088/0004-637X/815/2/82>. [arXiv:1508.03133](https://arxiv.org/abs/1508.03133) [astro-ph.HE]
163. M. Tanaka, D. Kato, G. Gaigalas, K. Kawaguchi, Systematic Opacity Calculations for Kilonovae. *Mon. Not. Roy. Astron. Soc.* **496**(2), 1369–1392 (2020). <https://doi.org/10.1093/mnras/staa1576>. [arXiv:1906.08914](https://arxiv.org/abs/1906.08914) [astro-ph.HE]
164. E. Nakar, T. Piran, Radio Remnants of Compact Binary Mergers - the Electromagnetic Signal that will follow the Gravitational Waves. *Nature* **478**, 82–84 (2011). <https://doi.org/10.1038/nature10365>. [arXiv:1102.1020](https://arxiv.org/abs/1102.1020) [astro-ph.HE]
165. K. Hotokezaka, T. Piran, Mass ejection from neutron star mergers: different components and expected radio signals. *Mon. Not. Roy. Astron. Soc.* **450**, 1430–1440 (2015). <https://doi.org/10.1093/mnras/stv620>. [arXiv:1501.01986](https://arxiv.org/abs/1501.01986) [astro-ph.HE]
166. K. Hotokezaka, S. Nissanke, G. Hallinan, T.J.W. Lazio, E. Nakar, T. Piran, Radio Counterparts of Compact Binary Mergers detectable in Gravitational Waves: A Simulation for an Optimized Survey. *Astrophys. J.* **831**(2), 190 (2016). <https://doi.org/10.3847/0004-637X/831/2/190>. [arXiv:1605.09395](https://arxiv.org/abs/1605.09395) [astro-ph.HE]
167. M. Haddadi, M.D. Duez, F. Foucart, T. Ramirez, R. Fernández, A.L. Knight, J. Jesse, F. Hébert, L.E. Kidder, H.P. Pfeiffer, M.A. Scheel, Late-time post-merger modeling of a compact binary: effects of relativity, *r*-process heating, and treatment of transport. *Class. Quant. Grav.* **40**(8), 085,008 (2023). <https://doi.org/10.1088/1361-6382/acc0c6>. [arXiv:2208.02367](https://arxiv.org/abs/2208.02367) [gr-qc]
168. F. Foucart, P. Moesta, T. Ramirez, A.J. Wright, S. Darbha, D. Kasen, Estimating out-flow masses and velocities in merger simulations: Impact of *r*-process heating and neutrino cooling. *Phys. Rev. D* **104**(12), 123,010 (2021). <https://doi.org/10.1103/PhysRevD.104.123010>. [arXiv:2109.00565ZZ](https://arxiv.org/abs/2109.00565ZZ) [astro-ph.HE]
169. K. Kyutoku, K. Ioka, M. Shibata, Anisotropic mass ejection from black hole-neutron star binaries: Diversity of electromagnetic counterparts. *Phys. Rev.* **D88**(4), 041,503 (2013). <https://doi.org/10.1103/PhysRevD.88.041503>. [arXiv:1305.6309](https://arxiv.org/abs/1305.6309) [astro-ph.HE]
170. S. Rosswog, Mergers of neutron star black hole binaries with small mass ratios: Nucleosynthesis, gamma-ray bursts and electromagnetic transients. *Astrophys. J.* **634**, 1202 (2005). <https://doi.org/10.1086/497062>. [arXiv:astro-ph/0508138](https://arxiv.org/abs/astro-ph/0508138) [astro-ph]
171. L.F. Roberts, J. Lippuner, M.D. Duez, J.A. Faber, F. Foucart, J.C. Lombardi, S. Ning, C.D. Ott, M. Ponce, The influence of neutrinos on *r*-process nucleosynthesis in the ejecta of black

- hole–neutron star mergers. *Mon. Not. Roy. Astron. Soc.* **464**(4), 3907–3919 (2017). <https://doi.org/10.1093/mnras/stw2622>. [arXiv:1601.07942](https://arxiv.org/abs/1601.07942) [astro-ph.HE]
172. R. Fernández, B.D. Metzger, Delayed outflows from black hole accretion tori following neutron star binary coalescence. *Mon. Not. Roy. Astron. Soc.* **435**, 502 (2013). <https://doi.org/10.1093/mnras/stt1312>. [arXiv:1304.6720](https://arxiv.org/abs/1304.6720) [astro-ph.HE]
173. R. Fernández, D. Kasen, B.D. Metzger, E. Quataert, Outflows from accretion discs formed in neutron star mergers: effect of black hole spin. *Mon. Not. Roy. Astron. Soc.* **446**, 750–758 (2015). <https://doi.org/10.1093/mnras/stu2112>. [arXiv:1409.4426](https://arxiv.org/abs/1409.4426) [astro-ph.HE]
174. R. Fernández, F. Foucart, D. Kasen, J. Lippuner, D. Desai, L.F. Roberts, Dynamics, nucleosynthesis, and kilonova signature of black hole–neutron star merger ejecta. *Class. Quant. Grav.* **34**(15), 154,001 (2017). <https://doi.org/10.1088/1361-6382/aa7a77>. [arXiv:1612.04829](https://arxiv.org/abs/1612.04829) [astro-ph.HE]
175. R. Fernández, F. Foucart, J. Lippuner, The landscape of disc outflows from black hole–neutron star mergers. *Mon. Not. Roy. Astron. Soc.* **497**(3), 3221–3233 (2020). <https://doi.org/10.1093/mnras/staa2209>. [arXiv:2005.14208](https://arxiv.org/abs/2005.14208) [astro-ph.HE]
176. S. Fujibayashi, M. Shibata, S. Wanajo, K. Kiuchi, K. Kyutoku, Y. Sekiguchi, Viscous evolution of a massive disk surrounding stellar-mass black holes in full general relativity. *Phys. Rev. D* **102**, 123,014 (2020). <https://doi.org/10.1103/PhysRevD.102.123014>. [arXiv:2009.03895](https://arxiv.org/abs/2009.03895) [astro-ph.HE]
177. S. Fujibayashi, M. Shibata, S. Wanajo, K. Kiuchi, K. Kyutoku, Y. Sekiguchi, Mass ejection from disks surrounding a low-mass black hole: Viscous neutrino-radiation hydrodynamics simulation in full general relativity. *Phys. Rev. D* **101**, 083,029 (2020). <https://doi.org/10.1103/PhysRevD.101.083029>. URL <https://link.aps.org/doi/10.1103/PhysRevD.101.083029>
178. M. Tanaka, K. Hotokezaka, K. Kyutoku, S. Wanajo, K. Kiuchi, Y. Sekiguchi, M. Shibata, Radioactively Powered Emission from Black Hole-Neutron Star Mergers. *Astrophys. J.* **780**, 31 (2014). <https://doi.org/10.1088/0004-637X/780/1/31>. [arXiv:1310.2774](https://arxiv.org/abs/1310.2774) [astro-ph.HE]
179. S. Darbha, D. Kasen, F. Foucart, D.J. Price, Electromagnetic Signatures from the Tidal Tail of a Black Hole-Neutron Star Merger. *Astrophys. J.* **915**(1), 69 (2021). <https://doi.org/10.3847/1538-4357/abff5d>. [arXiv:2103.03378](https://arxiv.org/abs/2103.03378) [astro-ph.HE]
180. S. Darbha, D. Kasen, Inclination Dependence of Kilonova Light Curves from Globally Aspherical Geometries. *Astrophys. J.* **897**(2), 150 (2020). <https://doi.org/10.3847/1538-4357/ab9a34>. [arXiv:2002.00299](https://arxiv.org/abs/2002.00299) [astro-ph.HE]
181. K. Kawaguchi, M. Shibata, M. Tanaka, Diversity of Kilonova Light Curves. *Astrophys. J.* **889**(2), 171 (2020). <https://doi.org/10.3847/1538-4357/ab61f6>. [arXiv:1908.05815](https://arxiv.org/abs/1908.05815) [astro-ph.HE]